

Modeling Pulsar Trajectories Through a  
Galactic Potential to Determine Birth Locations

By

Brent Shapiro-Albert

\*\*\*\*\*

Submitted in partial fulfillment  
of the requirements for  
Honors in the Department of Physics and  
Astronomy

UNION COLLEGE

March 2016

## ABSTRACT

SHAPIRO-ALBERT, BRENT Modeling Pulsar Trajectories Through a Galactic Potential to Determine Birth Locations. Department of Physics and Astronomy, March 2016

ADVISOR: Gregory Hallenbeck

Neutron stars are the remnants of massive stars after their deaths in supernova explosions. Some neutron stars, called pulsars, are detected as periodic emitters of radio waves at very precise intervals. Pulsars typically have higher velocities than their progenitor stellar population due to either kicks from supernova asymmetries or from remnant velocities of compact binaries after they are disrupted by explosions. Their velocities are large enough that pulsars will typically move large distances from their birth sites. By determining a pulsar's present day location and velocity, we project back to twice the pulsar's characteristic age to constrain the location of the progenitor star within the uncertainty of the unknown line-of-sight velocity component.

Previous research by Hoogerwerf et al. (2001), Vlemmings et al. (2004), and Kirsten et al. (2015) has traced back two pairs of objects, the pulsars B2020 + 28 and B2021 + 51, and the pulsar and runaway star B1929 + 10 and  $\zeta$ -Ophiuchi to determine their birth locations and found each pair was associated in some way. Using a Python implementation with the *Galpy* package, we replicate the results from this previous research and then project a new sample of 60 pulsars from the recent PSRPI survey back to determine their birth locations. The potential birth regions are a sample of 36 OB star associations selected from Tetzlaff et al. (2010). We also use this implementation to determine if there are any birth associations between two pulsars in our sample within the same region. We find that we can successfully model a pulsar's trajectory and determine a likely birth OB region for a pulsar with our model.

# Contents

<b>1</b>	<b>Introduction</b>	<b>1</b>
1.1	Velocities and Origin of Pulsars . . . . .	4
<b>2</b>	<b>Methods</b>	<b>7</b>
2.1	Data and Estimates . . . . .	7
2.1.1	Duration of Trajectories . . . . .	10
2.1.2	The Radial Velocity Distribution . . . . .	12
2.1.3	Determining Pulsar Birth Regions . . . . .	15
2.2	Computational Methods . . . . .	18
2.2.1	Implementation . . . . .	18
2.2.2	Using <i>Galpy</i> to Simulate Trajectories . . . . .	22
2.2.3	Initial Pair Tests . . . . .	23
<b>3</b>	<b>Initial Results</b>	<b>29</b>
3.1	$\zeta$ Ophiuchi and B1929+10 . . . . .	29
3.2	B2020+28 and B2021+51 . . . . .	32
<b>4</b>	<b>Results of PSRPI Trajectories</b>	<b>35</b>
4.1	Pulsar Pairs from the Same OB Region: J0102+6537 and J0357+5236 . . . . .	35
4.2	Pulsar Pairs with No OB Region Matches . . . . .	45
4.3	Pulsar Birth OB Regions: J0055+5117 and Cas OB2 . . . . .	46
<b>5</b>	<b>Conclusions</b>	<b>50</b>
<b>6</b>	<b>Appendix A</b>	<b>54</b>

# 1 Introduction

When a massive star dies in a supernova explosion, the inner core can collapse back into a white dwarf, a hot, dense star which is supported by electron degeneracy pressure. However, when the cores of these stars are very massive, the gravitational pressure overcomes the electron degeneracy pressure and the white dwarf collapses further. In this scenario, electrons and protons combine to form neutrons. These neutrons are packed so densely that there is no space between them. These extremely compact objects are called neutron stars and are supported by neutron degeneracy pressure (Hoyle et al., 1964). Some of these neutron stars rotate very rapidly and emit radio waves along their magnetic poles. Neutron stars that emit these radio waves are called pulsars, since as these neutron stars rotate, the radio waves they emit pass through our line of sight with a very precise period, creating a radio pulse.

Pulsars can be used as a laboratory to study extreme physics that we cannot replicate on Earth. We can study extreme magnetic environments on the order of  $10^8$  to  $10^{12}$  G. Neutron stars are also incredibly dense which allows us to perform tests of General Relativity (“GR”) and identify post-Keplerian corrections (Lorimer, 2008) to their orbits. In addition to these extreme environmental tests, pulsar binary pairs have been shown to be an indirect source of gravitational waves (Hulse & Taylor, 1975). It has also been theorized that we can directly detect these waves by long-term timing of a large array of pulsars (Jenet et al., 2009). If we have measurements of the motions of the pulsar we can also model its trajectory to try to find an associated supernova remnant (SNR) and learn more about pulsar birth supernovae (Dewey & Cordes, 1987, Vlemmings et al., 2004).

The first binary pulsar discovered was B1913 + 16, also known as the Hulse-Taylor binary. Careful study of this binary pulsar showed that the orbital period of the pulsar

and its invisible companion steadily decreased over time. Since GR predicts that the binary pair will radiate energy as gravitational waves, the system will lose energy over time and the orbital period will decrease as a result. The observed decrease in orbital period were found to match the predictions of GR (Hulse & Taylor, 1975). The amount of energy lost by the system is consistent with the amount of energy predicted to be lost due to gravitational wave emission, thus showing indirect evidence for gravitational waves (Hulse & Taylor, 1975).

Additionally, GR predicts orbits for close binary pairs which differ from the Keplerian orbits of Newtonian gravity. In a two-pulsar binary system, the magnetospheres can influence the radio pulses we see from each pulsar which allow us to measure the relativistic spin-orbital coupling (Graham-Smith & McLaughlin, 2005) which can also constrain predictions made by GR. Some binary orbits require corrections from GR, which come from equations utilizing “post-Keplerian” (PK) parameters (Lorimer, 2008). Depending on the observing conditions there are 19 different parameters that can be measured leading to 15 different tests of GR (Damour & Taylor, 1992). Since 1974 many pulsar binary tests of GR have occurred including further timing of B1913 + 16. This has shown that the decrease in orbital period of B1913 + 16 and its invisible companion agrees with the expected emission of gravitational waves, according to GR, to within 0.2% up to present day (Weisberg & Taylor, 2005). Other similar tests have been made in good agreement with the GR predictions (Jacoby et al., 2006, Stairs et al., 2002) and as instrumentation improves it is likely that more binary pulsars will be found and the number of GR tests will grow.

Pulsar periods can be measured using a baseline of a few months to an accuracy of around  $10^{-7}$  s or better (Jenet et al., 2009). Some pulsars, such as B1937 + 21, have been timed to an accuracy of  $10^{-13}$  s using a longer baseline of a few years (Davis et al., 1985).

The precision timing of pulsars can also be used to directly detect gravitational waves due to perturbations in the pulse periods from these waves. Theory predicts that by observing an ensemble of high-precision radio pulsars we will see fluctuations in the pulse arrival times from pulsars at nHz frequencies due to these gravitational waves. One group is the North American Nanohertz Observatory for Gravitational Waves (NANOGrav), which is a consortium of institutes and researchers using pulsar timing arrays which utilize pulsars as both a source of radio emission and a clock to time the radio pulses (Jenet et al., 2009). NANOGrav is also part of a global consortium along with the European Pulsar Timing Array (EPTA) and the Parkes Pulsar Timing Array (PPTA) which together form the International Pulsar Timing Array (IPTA). While the timing of many pulsars is better than 100 ns (Jenet et al., 2009), variation in the pulse arrival times from the Interstellar Medium (ISM), the pulsar itself, and the measurement process must be accounted for (Lam et al., 2015). Reducing the intrinsic pulse “jitter” and the observational noise, from factors such as the ISM, is a key step in direct detection of gravitational waves.

While pulsars have very strong magnetic fields, a particular class of pulsars called magnetars have magnetic fields between  $10^{14}$ - $10^{15}$  G. Magnetars are thus expected to be born in highly energetic supernovae with millisecond periods at birth (Duncan & Thompson, 1992). An alternative theory for magnetar birth is that the progenitor stars already have highly magnetic cores and the neutron stars formed during supernovae obtain large magnetic fields through magnetic flux conservation (Ferrario & Wickramasinghe, 2008). Current models underestimate the number of magnetars found in surveys thus far which poses a magnetar birthrate problem (Turolla et al., 2015). This suggests that we are not accounting for all of the possible ways a neutron star may acquire a magnetic field this strong. Magnetars are also observed to emit large flares in the X-ray. One explanation for these flares is sudden reconfigurations in the magnetosphere (Turolla et

al., 2015).

Pulsars with planets such as B1257 + 12 allow us to study the effects of extreme magnetic fields on planetary orbits and also allow us to constrain the birth parameters necessary to have a planet. B1257 + 12 was found to have a small magnetic field at birth, which suggests this is a necessary condition for a pulsar to have a planet (Cordes, 1993, Kohler, 2015).

## 1.1 Velocities and Origin of Pulsars

Pulsars are observed to have very large velocities perpendicular to our line of sight, or transverse velocity ( $V_{\perp}$ ), with many moving across the sky at speeds of a few hundred  $\text{km s}^{-1}$  (Gott et al., 1970). The pulsar B1508 + 55 has an observed transverse velocity of  $1083_{-90}^{+103} \text{ km s}^{-1}$  (Chatterjee et al., 2005), which is larger than the escape velocity of the galaxy. Examining the birth scenarios of pulsars gives insight into the origin of the large  $V_{\perp}$  that we observe. If we are able to determine the past trajectory of a pulsar in some cases it may be possible to determine a likely birth site or SNR. One theory behind these large  $V_{\perp}$  is asymmetric supernova “birth kicks” that would impart  $V_{\perp}$  of  $\sim 100 \text{ km s}^{-1}$ . (Chatterjee et al., 2005, Dewey & Cordes, 1987). However, in most models, this “kick” is not enough to give many pulsars the observed  $V_{\perp}$ , producing mostly  $V_{\perp} \leq 30 \text{ km s}^{-1}$  (Dewey & Cordes, 1987). In the case of B1508 + 55, a single asymmetric supernova was unable to account for the large  $V_{\perp}$ . Other theories, such as neutrino driven kicks within the supernova due to large magnetic fields on the order of  $10^{16} \text{ G}$  (Lai et al., 2001) or a disrupted binary system (Iben & Tutukov, 1996) were also found to be inadequate to produce a  $V_{\perp} > 1000 \text{ km s}^{-1}$ . Some combination of these mechanisms is concluded to be the most likely scenario, although no definite conclusions are drawn on how B1508 + 55

obtains its large  $V_{\perp}$ . We can further study the mechanisms behind these large  $V_{\perp}$  by tracing back the pulsar’s trajectory to determine where its progenitor star was located and examine possible pulsar birth scenarios.

One recent pulsar survey is Pulsar Parallax (PSRPI) which observed the parallax ( $\pi$ ) and proper motions ( $\mu$ ), the angular motion of a star across sky, of 60 pulsars using the Very Large Baseline Array (VLBA). All pulsars in this survey are within 4 kpc of the sun and all measurements of  $\mu$  and  $\pi$  had uncertainties less than 10%. The PSRPI survey has four goals: accurately measuring the distances to pulsars, improving Galactic electron density distribution models, associating pulsars with SNRs, and improving the ties between the International Celestial Reference Frame (ICRF), optical, and solar system barycenter frames (Deller et al., 2011). The results from PSRPI are thus essential in trying to map the galactic distribution of pulsars. Improving the distances and luminosities of these pulsars allow us to determine what the previous errors in distance and luminosity measurements may be. By correcting these errors, we can correct the pulsar distance and pulsar luminosity functions, which describe the galactic distribution of pulsars. To associate pulsars with SNRs, we need to simulate their trajectories which utilize  $\pi$  and  $\mu$  measurements (Deller et al., 2011). We can also estimate the distribution of pulsars across the galaxy, which allows us to examine the birth scenarios of these pulsars and better model large star supernovae. Since it is difficult to find pulsars because they are very faint, we know little about pulsars outside of the local population.

Although the large progenitor stars of pulsars generally have velocities of just a few 10’s of  $\text{km s}^{-1}$  we measure  $V_{\perp}$  in many pulsars to be a few 100’s of  $\text{km s}^{-1}$ . One motivation for determining birth locations of pulsars is to determine how pulsars obtain these much larger  $V_{\perp}$ . One prominent theory is that asymmetric SNe impart a birth “kick” to the neutron star that is formed at its core which gives the pulsar its large velocity (Dewey

& Cordes, 1987). If we can associate a pulsar with an SNR, then we can determine if the SNe is what imparted the large velocity to the pulsar, or if other factors may have contributed to it. However it is difficult to associate a pulsar with a particular SNR for a variety of reasons.

The focus of this work is to determine the birth locations of 60 pulsars from the PSRPI survey. In Chapter 2 we will discuss the problem posed by radial velocities ( $V_r$ ) and our estimated distributions of  $V_r$  for this distribution of pulsars (Hobbs et al., 2005). We will also discuss our pulsar trajectory model used to determine the birth locations of the PSRPI pulsars in Chapter 2. In Chapter 3 we will use our model to reproduce the results of Hoogerwerf et al. (2001), Vlemmings et al. (2004), and Kirsten et al. (2015) who determined the birth locations of two different pulsar pairs found to have a common origin, the runaway star  $\zeta$ -Ophiuchi and pulsar B1929+10 and the pulsar pair B2020+28 and B2021+51. We will then present the results of our model for all the PSRPI pulsars in Chapter 4.

## 2 Methods

### 2.1 Data and Estimates

The PSRPI survey observed 60 pulsars widely separated across the sky with the VLBA down to a detection limit of 1 mJy and measured parallaxes,  $\pi$ , to within  $\pm 25 \mu\text{as}$  and proper motions,  $\mu$ , to within  $\pm 25 \mu\text{as yr}^{-1}$ . This allows for  $V_{\perp}$  and distance measurements better than 10% at a distance of 4 kpc. Between 2011 and 2013, 84 hours were used in a preliminary survey of 245 pulsars. 60 pulsars were selected for further astrometric observations based on the number of sufficiently bright in-beam calibration sources (Deller et al., 2011). Another 690 hours were spent on 285 astrometric observations of the 60 pulsars of interest. Currently, a second survey focusing on millisecond pulsars, MSPSRPI, is underway. Our data come solely from the precursor PSRPI sample. The pulsars of the PSRPI survey as well as their present day positions, and characteristic ages can be found in Table 1. We do not report the  $\mu$  or  $\pi$  values because they are currently embargoed from publication. These values will be reported in Deller et al. (in prep).

Table 1  
PSRPI Pulsars

Pulsar	RA (J2000.0)	DEC (J2000.0)	$\tau$ (Myr)
J0040+5716	00 40 32.3857	57 16 24.838	6.15
J0055+5117	00 55 45.3968	51 17 24 621	3.51
J0102+6537	01 02 32.9905	65 37 13.413	4.47
J0108+6608	01 08 22.5110	66 08 34.457	1.56
J0147+5922	01 47 44.6449	59 22 03.281	10.21
J0151-0635*	01 51 22.7174	-06 35 02.981	52.4

Pulsar	RA (J2000.0)	DEC (J2000.0)	$\tau$ (Myr)
J0152-1637	01 52 10.8539	-16 37 53.597	10.2
J0157+6212	01 57 49.9431	62 12 26.616	0.197
J0323+3944*	03 23 26.6594	39 44 52.435	75.6
J0332+5434**	03 32 59.4071	54 34 43.341	5.53
J0335+4555*	03 35 16.6420	45 55 53.450	580
J0357+5236	03 57 44.8392	52 36 57.502	6.55
J0406+6138	04 06 30.0793	61 38 41.384	1.69
J0601-0527 <sup>†</sup>	06 01 58.9755	-05 27 50.847	4.82
J0614+2229	06 14 17.0055	22 29 56.849	0.0893
J0629+2415	06 29 05.7271	24 15 41.549	3.78
J0729-1836	07 29 32.3378	-18 36 42.255	0.426
J0823+0159*	08 23 09.7652	01 59 12.466	131
J0826+2637	08 26 51.5024	26 37 21.385	4.92
J1022+1001*	10 22 57.9963	10 01 52.760	60.2
J1136+1551	11 36 03.1234	15 51 13.893	5.04
J1257-1027	12 57 04.7626	-10 27 05.555	27.0
J1321+8323	13 21 45.6636	83 23 39.396	18.7
J1532+2745	15 32 10.3643	27 45 49.606	22.9
J1543-0620	15 43 30.1390	-06 20 45.323	12.8
J1607-0032	16 07 12.0619	-00 32 41.500	21.8
J1623-0908	16 23 17.6598	-09 08 48.853	7.84
J1645-0317	16 45 02.0408	-03 17 57.834	3.45
J1650-1654**	16 50 27.1700	-16 54 42.269	8.66

Pulsar	RA (J2000.0)	DEC (J2000.0)	$\tau$ (Myr)
J1703-1846	17 03 51.0913	-18 46 14.872	7.36
J1735-0724	17 35 04.9730	-07 24 52.155	5.47
J1741-0840	17 41 22.5628	-08 40 31.717	14.2
J1754+5201	17 54 22.9072	52 01 12.241	24.2
J1820-0427	18 20 52.5935	-04 27 37.728	1.5
J1833-0338	18 33 41.8955	-03 39 04.270	0.262
J1840+5640	18 40 44.5407	56 40 54.877	17.5
J1901-0906	19 01 53.0091	-09 06 11.133	17.2
J1912+2104	19 12 43.3396	21 04 33.930	3.48
J1913+1400	19 13 24.3529	14 00 52.564	10.3
J1917+1353	19 17 39.7864	13 53 57.073	0.428
J1919+0021	19 19 50.6711	00 21 39.721	2.63
J1937+2544	19 37 01.2550	25 44 13.446	4.95
J2006-0807*	20 06 16.3653	-08 07 02.159	200
J2010-1323*	20 10 45.9209	-13 23 56.081	1.72e4
J2046-0421	20 46 00.1723	-04 21 26.254	16.7
J2046+1540*	20 46 39.3378	15 40 33.557	98.9
J2113+2754	21 13 04.3524	27 54 01.207	7.27
J2113+4644	21 13 24.3287	46 44 08.836	22.5
J2145-0750*	21 45 50.4591	-07 50 18.513	8.54e3
J2149+6329	21 49 58.7018	63 29 44.271	35.8
J2150+5247 <sup>†</sup>	21 50 37.7493	52 47 49.559	0.521
J2212+2933*	22 12 23.3448	29 33 05.418	32.1

Pulsar	RA (J2000.0)	DEC (J2000.0)	$\tau$ (Myr)
J2225+6535**	22 25 52.8448	65 35 36.275	1.12
J2248-0101	22 48 26.8864	-01 01 48.071	11.5
J2305+3100	23 05 58.3214	31 00 01.291	8.63
J2317+1439	23 17 09.2364	14 39 31.261	2.26e4
J2317+2149*	23 17 57.8414	21 49 48.019	21.9
J2325+6316	23 25 13.3204	63 16 52.362	8.05
J2346-0609	23 46 50.4960	-06 09 59.884	13.7
J2354+6155	23 54 04.7808	61 55 46.840	0.92

Table 1: The sample of 60 pulsars from PSRPI. We have included the coordinates in RA and Dec (J2000.0) from the PSRPI project web page. It also includes the characteristic ages of each pulsar in Myr from the PSRCAT database. A “\*” denotes that the pulsar is too old to be accurately traced back. A “\*\*” denotes that data were not received in the final results. A “†” denotes an unresolved issue that led to an inability to accurately trace the pulsar back in time.

### 2.1.1 Duration of Trajectories

One estimate of a pulsar’s age is its characteristic age,  $\tau$ . We will reproduce the common derivation of  $\tau$  here. This is done by assuming that any change in the pulsar’s magnetic field strength and angle of inclination is negligible. We also assume that the pulsar’s current period is much longer than its birth period. We will represent the present day period by  $P$  and the initial period be  $P_0$ . We know from observations that the periods of pulsars change (Richards & Comella, 1969). By definition, the change rate of change in the period is

$$\dot{P} \equiv \frac{dP}{dt},$$

where  $\dot{P}$ , the first derivative of the period, is known as the “spin-down rate” of the pulsar.

We multiply both sides of the equation by the pulsar’s period  $P$  to get the equation

$$P\dot{P} = P\frac{dP}{dt}.$$

If we multiply both side of the equation by  $dt$ , we have the differential equation

$$P\dot{P}dt = PdP.$$

We then integrate the right hand side of the equation from the pulsar’s birth period,  $P_0$  to the pulsar’s present day period  $P$

$$\int_0^\tau P\dot{P}dt = \int_{P_0}^P PdP.$$

If we also assume that  $P\dot{P}$  for any given pulsar is constant over time (Taylor & Manchester, 1977), we can solve this differential equation by integrating the left hand side from the pulsars birth at time = 0 to the pulsar’s present day age, which we will call  $\tau$ .

$$P\dot{P}\tau = \frac{P^2 - P_0^2}{2}.$$

Now by our beginning assumption,  $P_0$  is much shorter than  $P$ . Thus  $P_0^2 \ll P^2$ , which simplifies our equation to

$$\frac{P^2}{2} = P\dot{P}\tau.$$

Now we can solve for the pulsar’s present day, or characteristic, age as

$$\tau = \frac{P}{2\dot{P}}. \tag{1}$$

However, since  $\tau$  is known to be imprecise and generally overestimate the pulsar’s age (Taylor & Manchester, 1977), we will trace each pulsar’s trajectory back to a maximum of  $2\tau$ .

Once pulsars have  $\tau$  more than a few 10’s of Myr old, other interactions that the pulsar may have had can change the values of  $\mu$  and  $\pi$  that a pulsar may have had at birth. We thus limit our study to younger pulsars with  $\tau \lesssim 30$  Myr. However there is a chance that these young pulsars have been “recycled.” These objects usually are older pulsars that have had their pulse periods sped-up again by accreting matter from a companion star, which increases their angular momentum (Tauris, 1994). These recycled pulsars often have millisecond periods which would lead to shorter inferred  $\tau$ . Recycled pulsars will also have different values of  $\mu$  and  $\pi$  than may have been observed at birth and so cannot be traced back (Bisnovatyi-Kogan, 2006). The PSRPI survey does not include any millisecond pulsars in order to try to avoid projecting back the trajectories of recycled pulsars. We cannot be sure that the pulsars in our sample were never part of a binary system. However since we know that none have millisecond periods, we know that none have been in a binary for at least the duration of their characteristic age. Thus we can still trace a pulsar back to its binary origin if not its actual birth OB region.

### 2.1.2 The Radial Velocity Distribution

We have now five of the six values needed to trace the trajectories of our pulsars, the pulsar’s position in RA and Dec,  $\mu$  (in RA and Dec), and  $\pi$ , from the PSRPI survey. The last value necessary to simulate the pulsar’s trajectory is  $V_r$ , the velocity along the line-of-sight, which we cannot measure. Since pulsars are not visible at optical wavelengths, we cannot determine  $V_r$  from the Doppler shift of known spectral lines. Instead we approximate  $V_r$  based on  $V_{\perp}$  measurements (Hobbs et al., 2005) to derive a Gaussian

probability density function (PDF) of possible values of  $V_r$  for any pulsar. The use of a Gaussian  $V_r$  Distribution is standard when simulating the trajectories of pulsars to determine their birth regions (Hoogerwerf et al., 2001, Kirsten et al., 2015). We use a previous analysis of 233 pulsars and their proper motions from Hobbs et al. (2005) to estimate  $V_r$ . This study derived a Maxwell-Boltzmann Distribution of three dimensional (3D) space velocities for pulsars.

While we cannot directly measure the 3D space velocity of a pulsar, we can generally measure the one or two dimensional space velocity. Since this observed data is consistent with an isotropic velocity vector, we can then obtain a 3D space velocity distribution from the 1D and 2D velocity measurements using a deconvolution technique (Hobbs et al., 2005). Hobbs et al. (2005) obtains two, one-sided 3D  $V_r$  Maxwell-Boltzmann Distributions, one from the 1D velocities and the other from the 2D velocities, with peaks at  $400 \text{ km s}^{-1}$  and  $431 \text{ km s}^{-1}$  respectively. These distribution are shown in Figures 1 and 2 and estimate the distribution of the unobservable  $V_r$  component.

However, since the pulsars can be moving towards us ( $V_r < 0$ ) or away from us ( $V_r > 0$ ), the distribution must include negative  $V_r$  values (Hoogerwerf et al., 2001, Vlemmings et al., 2004, Kirsten et al., 2015). Since Hobbs et al. (2005) determined a Maxwell-Boltzmann distribution which contains only positive velocities, we translate their distribution to determine a standard deviation ( $\sigma$ ) of this distribution and use it as the  $\sigma$  for a single Gaussian Distribution centered on  $0 \text{ km s}^{-1}$ . We determined  $\sigma$  to be  $578 \text{ km s}^{-1}$ . This allows us to make a direct comparison of our results with past results and minimize the amount of uncertainty between the different models. We use the Gaussian distribution in Figure 3 in our Monte Carlo simulations of the pulsar trajectories.

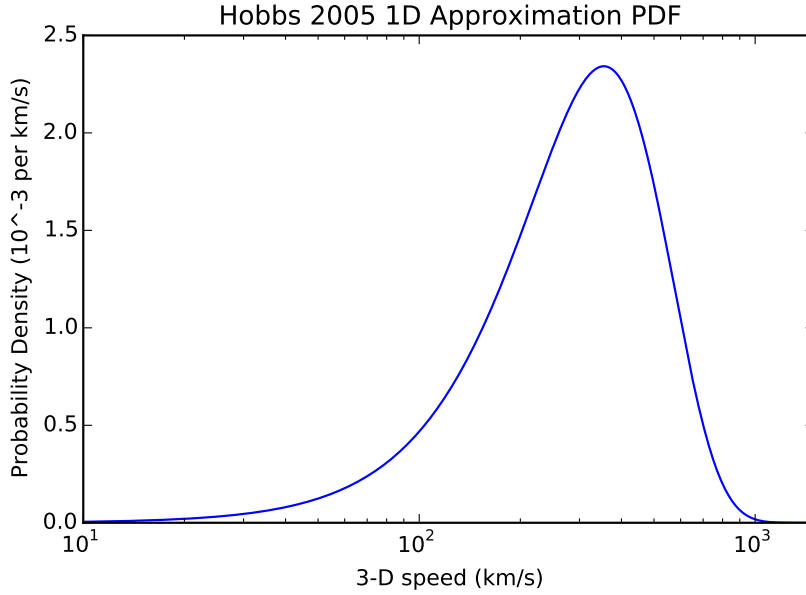


Figure 1: The 3D Maxwell-Boltzmann Distribution with a mean =  $400 \text{ km s}^{-1}$  and a standard deviation  $\sigma = 265 \text{ km s}^{-1}$ . This distribution is determined using the 1D velocity vectors of the pulsar sample from Hobbs et al. (2005). This distribution is used as the basis of the  $V_r$  probability density function (PDF) in Kirsten et al. (2015) as well as to derive the single Gaussian  $V_r$  PDF used in our model.

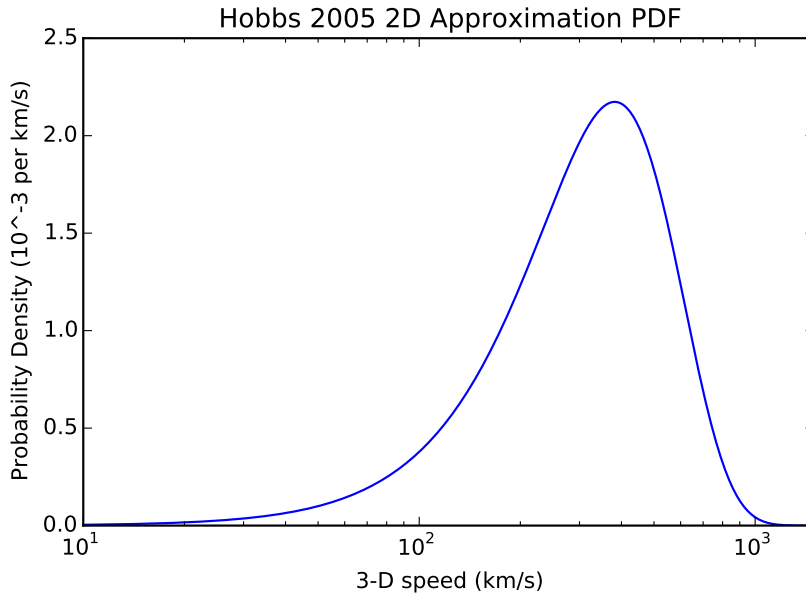


Figure 2: The 3D Maxwell-Boltzmann Distribution with a mean =  $431 \text{ km s}^{-1}$  and a standard deviation  $\sigma = 265 \text{ km s}^{-1}$ . This distribution is determined using the 2D velocity vectors of the pulsar sample from Hobbs et al. (2005).

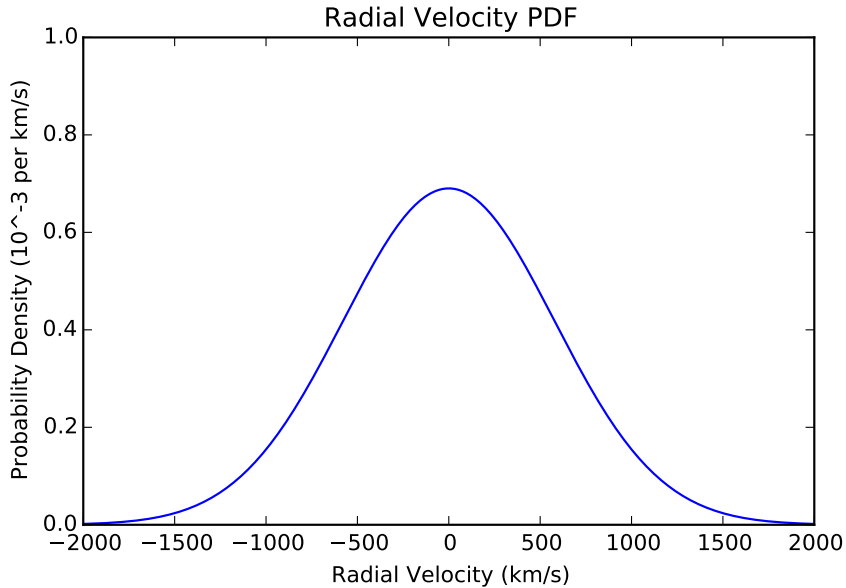


Figure 3: The Gaussian  $V_r$  PDF that we have derived from the PDF shown in Table 1. This distribution is centered an  $0 \text{ km s}^{-1}$  and has  $\sigma = 578 \text{ km s}^{-1}$ . This distribution allows us to account for negative values of  $V_r$ .

### 2.1.3 Determining Pulsar Birth Regions

Of the initial 60 pulsars only 46 have estimated ages below the upper limit  $\tau \lesssim 30$  Myr to avoid recycled pulsars. Additionally, we find 2 pulsars whose trajectories result in unrealistic trajectory clouds showing birth regions 100's to 1000's of kpc away from the Milky Way. The reason for this has yet to be resolved at the time of this writing. We therefore use a sample size of 44 pulsars for the remainder of this work. The pulsars that we do not use in our sample are denoted with a \*, \*\*, or † in Table 1. To determine the birth locations of these 44 pulsars we simulate their trajectories through a galactic potential. We do this using a Monte Carlo simulation, sampling each parameter,  $\pi$ ,  $\mu$ , and  $V_r$ , from Gaussian Probability Density Functions (PDFs) and generating 1750 potential orbits for each pulsar which form a 3D trajectory cloud. An example pair of clouds is

shown in Figure 4. We utilize the Python package *Galpy* (Bovy, 2015) to produce each trajectory. If it appears that we have overlapping trajectory clouds at the same time, as in Figure 4, we can compute the distance between the two pulsars for every possible pair of trajectories,  $\approx 3$  million. If we find that the pulsars are within 10 pc of each other at the same time, we define that pair of trajectories as “successful trajectories”.

OB star clusters and associations are clusters of stars with masses  $8 - 20 M_{\odot}$ . Since these regions are the most densely populated regions of stars large enough to produce a pulsar in a supernova, they are the most likely pulsar birth regions. We have selected 36 possible OB star clusters from Tetzlaff et al. (2010). Our 36 regions are widely distributed across the sky, similar to our sample of 60 pulsars. Included in our selection are OB star clusters that have previously been determined to be the birth region of pulsars (Hoogerwerf et al., 2001, Vlemmings et al., 2004, Tetzlaff et al., 2010). Since these regions are also moving in the Galaxy, similarly to how we trace back our pulsars, we need to trace back these regions to determine where they were located at the time of each pulsar’s birth. If we find that the trajectory clouds of one of our pulsars intersects with the trajectory clouds of one of these OB regions, we can determine the likelihood that the pulsar was actually born in that region. Similarly to our pulsar pairs, if we find that the pulsar and the OB region are within 10 pc of each other at the same time, we define that pair of trajectories as “successful trajectories”.

We use a different set of parameters to trace back the centers of these OB regions than we do for the pulsars. Whereas for a pulsar we use  $\mu$  and  $V_r$ , for an OB region we use the parameters of  $U$ ,  $V$ , and  $W$ , in  $\text{km s}^{-1}$ , where these are the 3D space velocity vectors according to the galactic coordinate system. We also have parallax measurements as well as estimates of the ages of each OB region and the present day coordinates of the centers of these OB regions. We have used these parameters as compiled by Tetzlaff et

al. (2010), from various sources found therein, and report them in Table 2.

Table 2  
OB Regions

Name	$l$ ( $^{\circ}$ )	$b$ ( $^{\circ}$ )	$\pi$ (mas)	$U$ (km s $^{-1}$ )	$V$ (km s $^{-1}$ )	$W$ (km s $^{-1}$ )	Age (Myr)
US	351.07	19.43	6.65	$-6.7 \pm 5.5$	$-16.0 \pm 3.5$	$-8.0 \pm 2.7$	10
UCL	330.51	12.86	6.96	$-6.8 \pm 4.6$	$-19.3 \pm 4.7$	$-5.7 \pm 2.5$	20
LCC	301.54	6.74	8.38	$-8.2 \pm 5.1$	$-18.6 \pm 7.3$	$-6.4 \pm 2.6$	20
TWA	291.61	20.22	16.46	$-9.7 \pm 4.1$	$-17.1 \pm 3.1$	$-4.8 \pm 3.7$	20
Tuc-Hor	296.57	-51.72	23.09	$-10.1 \pm 2.4$	$-20.7 \pm 2.3$	$-2.5 \pm 3.8$	40
$\beta$ Pic-Cap	330.95	-55.54	54.97	$-10.8 \pm 3.4$	$-15.9 \pm 1.2$	$-9.8 \pm 2.5$	34
$\epsilon$ Cha	300.43	-15.08	10.41	$-8.6 \pm 3.6$	$-18.6 \pm 0.8$	$-9.3 \pm 1.7$	15
$\eta$ Cha	292.42	-21.45	10.76	$-12.2 \pm 0.01$	$-18.1 \pm 0.9$	$-10.1 \pm 0.5$	8
HD 141569	7.40	39.50	9.94	$-5.4 \pm 1.5$	$-15.6 \pm 2.6$	$-4.4 \pm 0.8$	5
Ext. R CrA	359.41	-17.19	9.85	$-0.1 \pm 6.4$	$-14.8 \pm 1.4$	$-10.1 \pm 3.3$	15
AB Dor	146.31	-59.00	71.43	$-7.4 \pm 3.2$	$-27.4 \pm 3.2$	$-12.9 \pm 6.4$	30
Her-Lyr	180.00	68.20	52.10	$-13.6 \pm 3.7$	$-22.7 \pm 3.4$	$-7.9 \pm 5.2$	40
Sgr OB5	0.00	-1.19	0.41	$-6.5 \pm 10.8$	$1.2 \pm 11.6$	$1.3 \pm 15.0$	12
NGC 6530	6.07	-1.33	0.76	$-12.1 \pm 6.3$	$-16.2 \pm 1.0$	$-14.3 \pm 0.8$	5
Sgr OB4	12.10	-0.99	0.52	$1.7 \pm 3.6$	$-6.2 \pm 7.2$	$-7.3 \pm 12.8$	10
Ser OB1	16.73	0.00	1.88	$-4.3 \pm 4.9$	$-3.1 \pm 1.6$	$-2.1 \pm 1.3$	13
Sct OB2	23.21	-0.53	0.63	$-8.7 \pm 7.5$	$-7.8 \pm 8.1$	$-4.4 \pm 3.8$	6
NGC 6823	59.40	-0.15	0.43	$63.9 \pm 3.0$	$-18.0 \pm 1.8$	$-0.8 \pm 4.1$	7
NGC 6871	72.65	2.05	0.64	$49.5 \pm 1.9$	$-25.8 \pm 2.2$	$-10.4 \pm 2.0$	10
Cyg OB2	80.22	0.80	0.67	$28.5 \pm 1.7$	$-33.0 \pm 0.3$	$-11.4 \pm 1.8$	5
Cep OB1	104.19	-1.01	0.65	$41.7 \pm 1.6$	$-47.2 \pm 3.0$	$-1.9 \pm 1.5$	6
Cas OB2	112.13	0.02	0.48	$58.2 \pm 6.2$	$-24.9 \pm 12.5$	$-1.0 \pm 4.9$	10
NGC 457	126.65	-4.38	0.41	$42.7 \pm 2.5$	$-9.6 \pm 2.8$	$-23.1 \pm 2.0$	24
Cam OB3	146.95	2.88	0.29	$9.1 \pm 14.2$	$-37.4 \pm 17.5$	$13.5 \pm 8.2$	11
Pleiades	166.63	-23.47	7.69	$-6.4 \pm 0.3$	$-26.8 \pm 0.1$	$-13.6 \pm 0.2$	120

Name	$l$ ( $^{\circ}$ )	$b$ ( $^{\circ}$ )	$\pi$ (mas)	$U$ (km s $^{-1}$ )	$V$ (km s $^{-1}$ )	$W$ (km s $^{-1}$ )	Age (Myr)
Gem OB1	189.00	2.30	0.49	$-14.5 \pm 1.5$	$-16.9 \pm 2.9$	$-10.2 \pm 1.9$	9
Ori OB1	206.96	-17.53	2.43	$-20.9 \pm 0.8$	$-12.1 \pm 0.5$	$-6.7 \pm 0.5$	11
CMa OB1	224.60	-1.50	0.61	$-40.3 \pm 4.2$	$-4.6 \pm 4.1$	$-21.3 \pm 2.3$	3
Col 121	237.40	-7.74	1.29	$-37.4 \pm 1.5$	$-14.9 \pm 2.2$	$-13.9 \pm 0.8$	11
Vel OB2	262.41	-7.52	1.97	$-26.3 \pm 3.1$	$-19.8 \pm 2.7$	$-6.9 \pm 1.3$	10
Car OB1	286.50	-1.49	0.53	$-66.5 \pm 1.0$	$-15.0 \pm 1.6$	$-8.9 \pm 0.9$	12.5
Cru OB1	294.89	-1.08	0.61	$-43.7 \pm 1.6$	$-16.6 \pm 1.9$	$-6.2 \pm 0.8$	7
Cen OB1	304.18	1.41	0.56	$-45.5 \pm 1.3$	$-6.7 \pm 1.7$	$-8.2 \pm 1.7$	12
Ara OB1A	337.71	-0.92	0.89	$-16.0 \pm 8.3$	$-7.8 \pm 4.0$	$-11.6 \pm 2.1$	50
Sco OB1	343.74	1.36	0.65	$-29.4 \pm 2.8$	$-2.8 \pm 1.5$	$-5.8 \pm 1.5$	8
Sco OB4	352.40	3.44	0.91	$3.9 \pm 0.3$	$-8.5 \pm 0.8$	$-8.5 \pm 0.8$	7

Table 2: The 36 regions we have sampled from Tetzlaff et al. (2010) with parameters from various sources found therein. Each region is listed with its galactic latitude,  $l$ , and longitude,  $b$ , according to the J2000 coordinate system in degrees. The parallax measurements,  $\pi$ , the heliocentric velocity components  $U$ ,  $V$ , and  $W$  and the associated uncertainties along with their estimated ages.

## 2.2 Computational Methods

### 2.2.1 Implementation

In order to generate the 1750 trajectories for each pulsar, we need to choose a  $\mu$ ,  $\pi$ , and  $V_r$  for each trajectory. We randomly choose each of our four parameters from a Gaussian PDF of each parameter, centered on the measured value and with a  $\sigma$  equal to the uncertainty in each measurement. By randomly choosing each parameter within the PDF we are accounting for the uncertainties in these measurements which allows us to more accurately obtain results.

Our model utilizes not only the *Galpy* package, but also the *Astropy* package. These

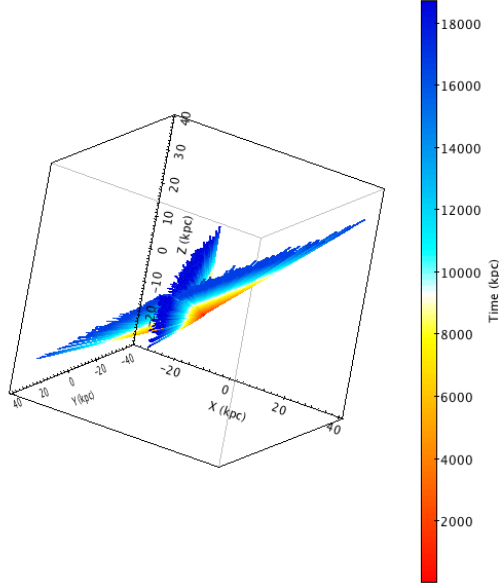


Figure 4: Two trajectory clouds using the pulsars J1321 + 8323 and J2046 – 0421. We see the two trajectory clouds overlapping at about the same time which suggests a common origin is possible. The x, y and z axes are in kpc as measured from the Galactic center (GC). Colors indicate time, where the time scale is in kyr backwards from the present, thus 1000 kyr is the same as being traced back for 1 Myr.

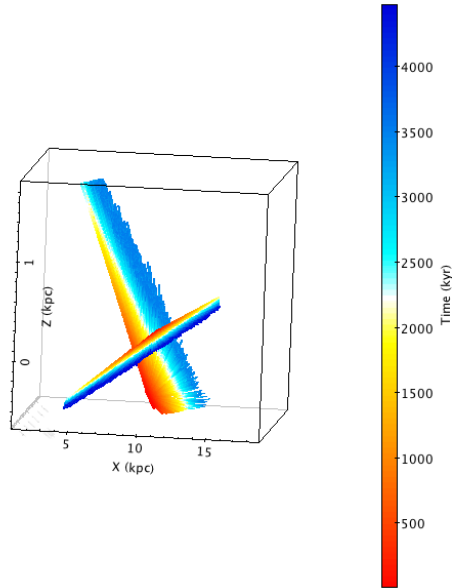


Figure 5: Two trajectory clouds using the pulsars J0055 + 5117 and J0102 + 6537. We see that while these clouds intersect, they do not intersect at the same time. The x, y and z axes are in kpc as measured from the GC. Colors indicate time, where the time scale is in kyr backwards from the present, thus 1000 kyr is the same as being traced back for 1 Myr.

packages are designed to both process large amounts of data and transform coordinates from Cartesian to galactic coordinates and ICRS RA and Dec coordinates. Our model reads the necessary input parameters and their associated uncertainties from a text file. This also includes the characteristic age,  $\tau$ , and the number of trajectories we want to generate. The number of time steps is calculated from the input  $\tau$  in such a way that we will retain the pulsars coordinates every  $10^3$  years. Using *Galpy* to generate 1750 random trajectories for one pulsar takes about 2 minutes and is thus very time efficient. The  $V_r$  PDF, our single Gaussian centered on  $0 \text{ km s}^{-1}$  with a  $\sigma = 578 \text{ km s}^{-1}$  as described above, is programmed directly into the code.

Once we have generated the trajectory clouds for our pulsars, we want to compute how close together a pair of pulsars was at the same time in their trajectories to see if they had a common origin. We can use another function built into our model to compare the distances of two pulsars for the duration of twice the characteristic age of the younger pulsar every  $10^3$  years. By plotting the trajectory clouds of the two pulsars, we can visually determine if they could have a common origin. Figure 4 shows two pulsars that could have a common origin, since they intersect at the same time. Figure 5 shows two pulsars that clearly intersect but at very different times, in this case about 2 Myr apart. They could have passed within 10 pc of each other at some point, but are not likely to have a common origin. If we find two pulsars that appear to have come from a common origin, as in Figure 4, we can compare the separation distance at every time step on every trajectory for one pulsar with the same time step on every trajectory on the other pulsar. With 1750 trajectories for each pulsar, we have  $1750^2 \approx 3$  million different possible orbital pairs. If the distance between the two pulsars being compared is 10 pc or less at the same time step, we record the minimum separation and the time that it occurs, as well as the parameters of the trajectories that generated this pair. Since  $\tau$  is only a rough estimate

of age, it is of interest to note all times where the separation is  $\leq 10$  pc. We use 10 pc as our maximum separation for a pair of successful trajectories consistent with previous studies (Hoogerwerf et al., 2001, Vlemmings et al., 2004, Kirsten et al., 2015).

To trace back the trajectories of the OB Star Clusters, we use the same method for the pulsars, utilizing *Galpy* and a Monte Carlo Method to generate 1750 trajectories. An example trajectory cloud for one of these OB associations is shown in Figure 6. When determining whether or not a pulsar could have come from a particular OB Cluster, we use the same distance comparison method, counting only those trajectories with separation of  $\leq 10$  pc between the pulsar and the center of these associations, consistent with Hoogerwerf et al. (2001).

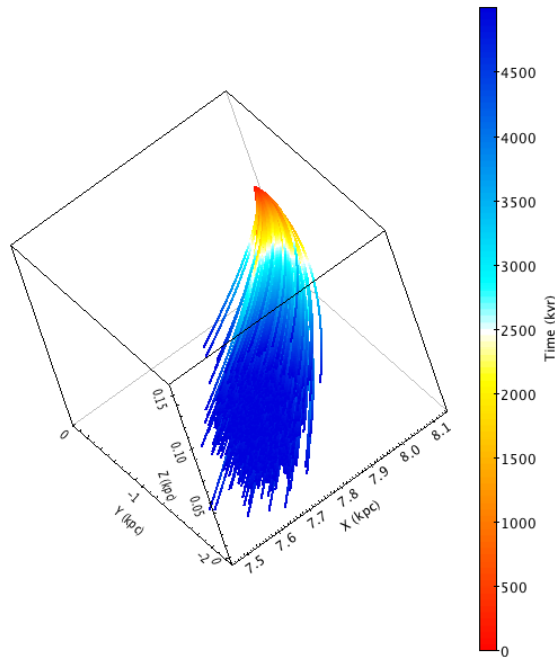


Figure 6: The trajectory cloud for the Upper Scorpius OB association. These OB association clouds are compared with pulsar trajectory clouds to determine if the pulsar could have been born there. The x, y and z axes are in kpc as measured from the GC. Colors indicate time, where the time scale is in kyr backwards from the present, so 1000 kyr is the same as being traced back for 1 Myr.

### 2.2.2 Using *Galpy* to Simulate Trajectories

The *Galpy* package (Bovy, 2015) integrates positions backwards based on present day parameters RA, Dec,  $\mu$  in RA ( $\mu_\alpha$ ) and Dec ( $\mu_\delta$ ), distance (d) from the Earth, and  $V_r$ . We also specify the distance Earth is from the Galactic center (GC), ( $R_o$ ). We use  $R_o = 8.27$  kpc from Schönrich (2012) and the rotation velocity of the galaxy at  $R_o$ , which we have specified as  $v_o = 219.7 \text{ km s}^{-1}$  from Vlemmings et al. (2004). We then can specify the correction for the 3D solar motion relative to the local standard of rest. We do this by specifying the 3D space velocity vectors according to the galactic coordinate system. These 3D vectors as labeled  $U$ ,  $V$ , and  $W$  respectively. We set  $U = 13.84$ ,  $V = 12.24$ , and  $W = 6.1 \text{ km s}^{-1}$  also from Schönrich (2012).

*Galpy* can also account for the Milky Way’s gravitational potential. In particular we use MWPotential2014, a composite potential with four different parts which is pre-compiled in *Galpy* (Bovy, 2015). The first part of this potential is a Miyamoto-Nagai Potential which accounts for the gravitational potential of the disk in the Milky Way (Miyamoto & Nagai, 1975). The second part is a Navarro-Frenk-White (NFW) Potential which is the gravitational potential due to the dark matter halo in the Milky Way (Navarro et al., 1996). The third component of MWPotential2014 is a power-law density spherical potential with an exponential cutoff (Bovy & Rix, 2013) which is the gravitational potential of the central bulge of the Milky Way. The fourth component is a Kepler Potential to account for the gravitational potential of the super massive black hole at the center of the Milky Way, Sgr A\*, which is modeled in the potential as a point source (Gillessen et al., 2009).

In order to determine if two pulsars were within 10 pc of each other at the same time in their trajectory, we want to make sure the pulsars do not move more than 10 pc at

every time step. For this reason we use time steps of  $10^3$  yrs from the present day position back through the trajectory to  $2\tau$  for all pulsars.

We override the default integrator in *Galpy* (“Scipy *odeint*”) and instead we use a Fourth Order Runge-Kutta integration method, consistent with Kirsten et al. (2015) and Hoogerwerf et al. (2001). When we compare the results of changing the integration method, we obtain a difference of  $\sim 15$  successful orbits. This is a difference in our success rate of only 0.0005%. We can therefore conclude that the method of integration does not make a large difference in the overall method. Using *Galpy* to integrate the orbits and then obtain the coordinates is not computationally expensive.

### 2.2.3 Initial Pair Tests

Since we are utilizing the new Python package *Galpy*, it is necessary to compare our model with previously published results. We thus attempt to replicate the results described in Hoogerwerf et al. (2001) of the runaway star  $\zeta$ -Ophiuchi and the pulsar B1929 + 10, as well as those described in Kirsten et al. (2015) for both the aforementioned pair and the pulsar pair B2020 + 28 and B2021 + 51. This pair of pulsars was initially analyzed by Vlemmings et al. (2004), whose results we also compare our model to.

#### $\zeta$ Ophiuchi and B1929+10

The pulsar and runaway star pair B1929 + 10 and  $\zeta$ -Ophiuchi was first analyzed by Hoogerwerf et al. (2001). These objects were originally traced back to a common origin in the Upper Scorpius region approximately 1 Myr ago (Hoogerwerf et al., 2001).  $\zeta$ -Ophiuchi was previously found to have been a runaway star located in the Upper Scorpius Sco OB2 region about 1 Myr ago by de Zeeuw et al. (1999) who inferred that a supernova forced

$\zeta$ -Ophiuchi out of this region. Hoogerwerf et al. (2001) found that the pulsar B1929 + 10 also passed by the Upper Scorpius Sco OB2 region about 1 – 2 Myr ago. Trajectory projections for the 9 pulsars analyzed by Hoogerwerf et al. (2001) are shown in Figure 7 which, along with the caption, has been reproduced here from Hoogerwerf et al. (2001). The pulsar B1929 + 10, referred to by Hoogerwerf et al. (2001) as J1932 + 1059, is labeled “8.”

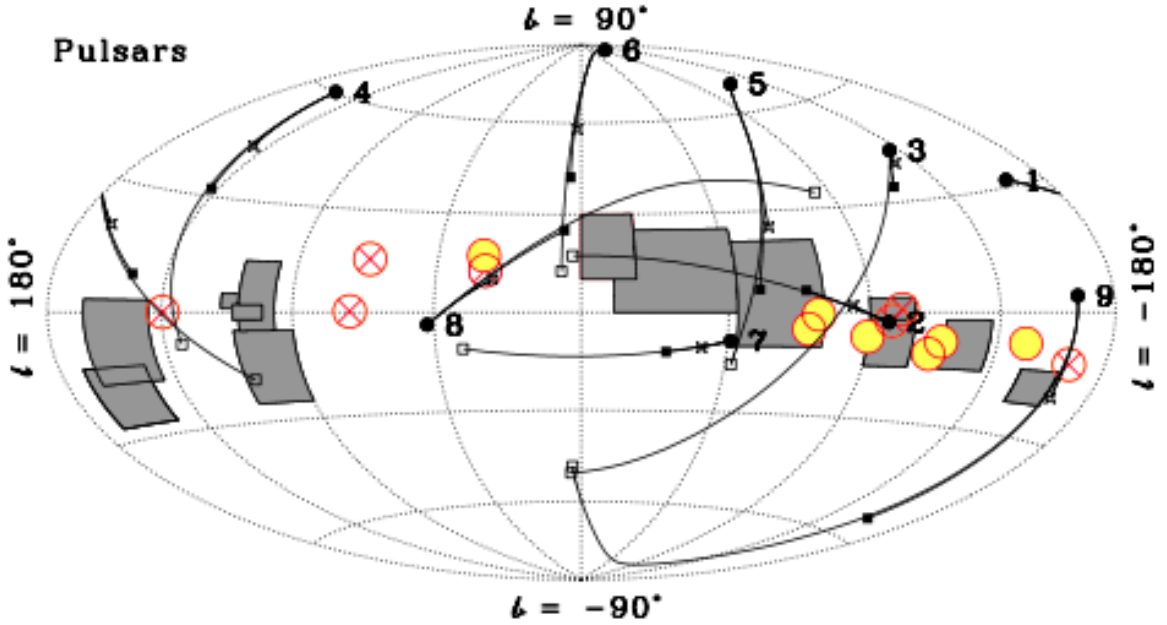


Figure 7: Pulsar sample defined in Sect. 2.1 [of Hoogerwerf et al. (2001)], in Galactic coordinates. The filled circles indicate the present position of the pulsars. The past orbits of pulsars, calculated for 2 Myr, are shown for three different assumed radial velocities:  $0 \text{ km s}^{-1}$  (filled squares),  $200 \text{ km s}^{-1}$  (open squares),  $-200 \text{ km s}^{-1}$  (open stars). The pulsars are labeled 1 through 8; 1: J0826 + 2637, 2: J0835 – 4510 (Vela pulsar), 3: JJ0953 + 0755, 4: J1115 + 5030, 5: J1136 + 1551, 6: J1239 + 2453, 7: J1456 – 6843, 8: J1932 + 1059. Number 9 is the neutron star Geminga. The associations and open cluster typically move comparatively little in 2 Myr.

Since these two objects were both located around the same star forming region at about the same time, the pulsar is a good candidate for being associated with the supernova responsible for forcing out  $\zeta$ -Ophiuchi. Hoogerwerf et al. (2001) adopted a  $V_r$

distribution of  $200 \pm 50 \text{ km s}^{-1}$  for the pulsar. They also doubled the uncertainties associated with the proper motions (Taylor et al., 1993) due to a possibility that they had been underestimated (Campbell et al., 1996). Using the same Monte Carlo method we have described, they simulated 3 million possible pairs of orbits for the two objects. In addition to comparing the distance between the two objects, they also traced back the trajectory of the Sco OB2 region and compared the distance of the two objects to the center of this association.

In addition to Hoogerwerf et al. (2001), Kirsten et al. (2015) performed the same Monte Carlo simulation on B1929 + 10 and  $\zeta$ -Ophiuchi using the same parameters. They also adopted a galactic potential using the three part Staekel potential (Famaey & Dejonghe, 2003) and solar motions from Schönrich (2012). *Galpy* does not have a Staekel potential option, but it does have a Kuzmin-Kutuzov Staekel potential, which is a Galactic potential which accounts for three integrals of motion (Dejonghe & de Zeeuw, 1988). We initialize an approximate three part Staekel Potential in *Galpy* by setting three individual KuzminKutuzovStaekel potential objects and put them together in one list and then use this list to make our galactic potential. This simulation by Kirsten et al. (2015) was completed as part of a consistency check with Hoogerwerf et al. (2001) to attempt to use the most recent, accurate measurements of the parameters of B1929 + 10 and  $\zeta$ -Ophiuchi to verify the initial results of Hoogerwerf et al. (2001).

Kirsten et al. (2015) also obtained new measurements for the parameters used to trace  $\zeta$ -Ophiuchi (van Leeuwen, 2007) and new astrometric parameters for B1929 + 10 (Kirsten et al., 2015) and compared the past results described above with those obtained with the most recent astrometric values. Here, they use the same solar motions and galactic potential as described above, but they adopt a bimodal  $V_r$  distribution for the pulsar with peaks centered on  $\pm 400 \text{ km s}^{-1}$  and standard deviations from these peaks

of  $265 \text{ km s}^{-1}$  shown in Figure 8. We adopt the same distribution picking the positive and negative values by randomly picking values for  $V_r$  from a Gaussian centered on  $400 \text{ km s}^{-1}$  with  $\sigma = 265 \text{ km s}^{-1}$  and then randomly assigning 50% of them a negative sign. Kirsten et al. (2015) found that using the most recent astrometric measurements, it is possible that their paths may have been close to each other about 0.5 Myr ago, but it is unlikely that the two objects had either a common origin or originated in the Upper Scorpius region.

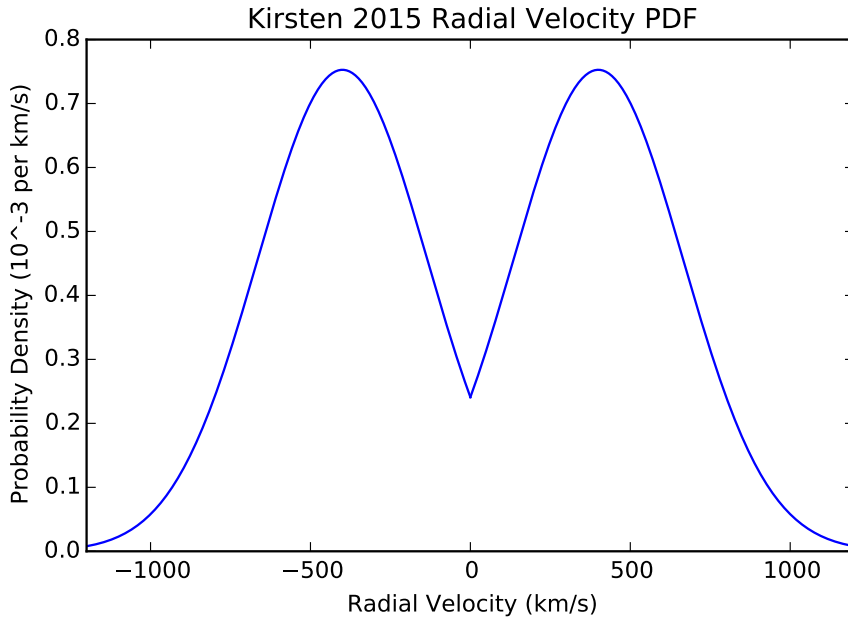


Figure 8: A bimodal  $V_r$  PDF used by Kirsten et al. (2015) in their Monte Carlo pulsar trajectory simulations of the pulsars B1929 + 10, B2020 + 28, and B2021 + 51. They use a Gaussian PDF centered on  $400 \text{ km s}^{-1}$  with  $\sigma = 265 \text{ km s}^{-1}$  and then randomly assign a positive or negative value to the chosen value. This is equivalent to selecting a  $V_r$  from the bimodal distribution shown here.

## B2020+28 and B2021+51

We now consider the pair of pulsars, B2020 + 28 and B2021 + 51. These pulsars were first traced back to a common origin within the Cygnus superbubble, near the Cyg OB2 region, approximately 2 Myr ago (Vlemmings et al., 2004). The characteristic ages of B2020 + 28 and B2021 + 51 are 2.87 and 2.74 Myr respectively, which are both close to 2 Myr. This pair is particularly interesting because the directions of the trajectories of these two pulsars is directly opposite each other. This suggests that the progenitor stars of these two pulsars were originally in a binary system with each other, which was disrupted when the second star went supernova and the two resulting pulsars were sent shooting away from each other (Vlemmings et al., 2004). We know that this cannot have happened after the first supernova because the pulsars have a similar  $\tau$ . This birth scenario is shown in Figure 9 which has been reproduced, along with its caption, from Vlemmings et al. (2004).

We attempted, but were unsuccessful, to replicate the radial velocity PDFs for the two pulsars from the information given in Vlemmings et al. (2004) due to a lack of description on the methods used to calculate the curves. However Vlemmings et al. (2004) reports the peaks of the PDFs for B2020 + 28 and B2021 + 51 to be  $\pm 100 \text{ km s}^{-1}$  and  $\pm 450 \text{ km s}^{-1}$  respectively. We thus estimate the  $V_r$  PDFs with a bimodal Gaussian with peaks at  $\pm 100 \text{ km s}^{-1}$  for B2021 + 51 and a similar type of PDF for B2020 + 28 but with peaks at  $\pm 450 \text{ km s}^{-1}$ . We then use our Monte Carlo Method to determine the number of successful trajectories for B2020 + 28 and B2021 + 51.

In addition to analyzing the trajectories of B1929 + 10 and  $\zeta$ -Ophiuchi, Kirsten et al. (2015) also studied B2020 + 28 and B2021 + 51 since they had new astrometric measurements for the pulsars. They again use the three-part Staekel Potential described

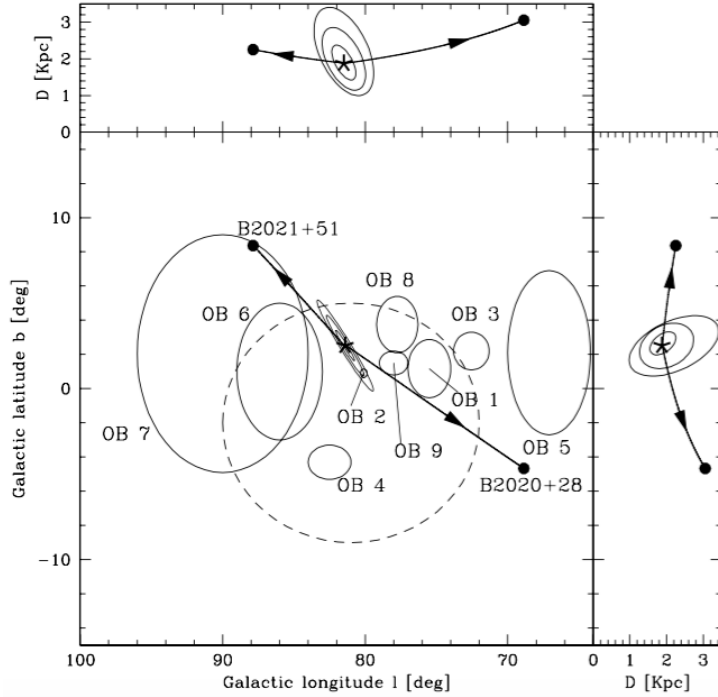


Figure 9: Three-dimensional pulsar motion through the Galactic potential for one of the pulsar orbit solutions that yields a minimum separation of less than 10 pc (these particular Galactic orbits cross within 4 pc). The dashed circle represents the CSB [Cygnus superbubble], while the labeled solid ellipses are the Cyg OB associations with positions and extents as tabulated by Uyaniker et al. (2001). The extent of OB 2 is unknown, and only the center of the association is indicated. The thick solid lines indicate the pulsar paths, with the origin denoted by the star and the arrows pointing in the direction of motion. The current positions are indicated by the filled circles. The elliptical contours around the pulsars' origin in these panels indicate the 1, 2, and 3  $\sigma$  levels of the likelihood solution for the birth location for Galactic orbit solutions that reach a minimum separation of less than 10 pc.

earlier. They use the same radial velocity distribution as in the previous simulation with B1929 + 10 and  $\zeta$ -Ophiuchi, shown in Figure 8. Their recent results suggest that B2020 + 28 and B2021 + 51 were not born inside the Cygnus superbubble, but somewhere outside of it, and gives the pulsars a much earlier time of closest approach, about  $1.16^{+0.18}_{-0.17}$  Myr ago. However they do not completely rule out a common origin for the two objects.

### 3 Initial Results

While we do not have new astrometric parameters for the pairs B1929 + 10 and  $\zeta$ -Ophiuchi and B2020 + 28 and B2021 + 51, we are interested in replicating the previous results to verify our analysis method before using it to trace back the trajectories of the 44 PSRPI pulsars and determine their birth regions. In this section we present our results in replicating the simulations done in Hoogerwerf et al. (2001), Vlemmings et al. (2004), and Kirsten et al. (2015).

#### 3.1 $\zeta$ Ophiuchi and B1929+10

We first present the results of our replication of the B1929 + 10 and  $\zeta$ -Ophiuchi simulations. The  $\pi$  and  $\mu$  values used to determine the trajectories for B1929 + 10 and  $\zeta$ -Ophiuchi are shown in Table 3. The parameters used for determining the trajectories of this OB region, the Upper Scorpius region, (de Zeeuw et al., 1999) are shown in Table 2 denoted with the name “US”. We present a comparison of all of the simulations completed with all three sets of parameters in Table 4. These three set of parameters are those from Hoogerwerf et al. (2001), van Leeuwen (2007), and Kirsten et al. (2015). The table presents the number of separations of  $\leq 10$  pc between B1929 + 10 and  $\zeta$ -Ophiuchi as well as the number and percentage of successful trajectories to total trajectories between B1929 + 10 and  $\zeta$ -Ophiuchi and the Upper Scorpius (US) region.

Table 3  
Astrometric Parameters for B1929 + 10 and  $\zeta$ -Ophiuchi

Name	RA (J2000)	Dec (J2000)	$\mu_\alpha$ (mas yr <sup>-1</sup> )	$\mu_\delta$ (mas yr <sup>-1</sup> )	$\pi$ (mas)	Dist (kpc)	$\tau$ (Myr)
B1929 + 10 <sup>a</sup>	19 32 14.021289	10.59 32.90137	99.0 ± 12.0	39.0 ± 8.0	4.00 ± 2.0	0.24 <sup>+0.09</sup> <sub>-0.12</sub>	3.1
B1929 + 10 <sup>b</sup>	19 32 14.021289	10.59 32.90137	94.08 ± 0.17	43.25 ± 0.16	2.77 ± 0.08	0.36 ± 0.11	3.1
$\zeta$ -Ophiuchi <sup>a</sup>	16 37 09.53	-10 34 01.7	13.07 ± 0.85	25.44 ± 0.72	7.12 ± 0.71	0.14 ± 0.01	N/A
$\zeta$ -Ophiuchi <sup>c</sup>	16 37 09.53	-10 34 01.7	15.26 ± 0.26	24.79 ± 0.22	8.91 ± 0.20	0.11 ± 0.01	N/A

Table 3: Astrometric parameters for B1929 + 10 and the runaway star  $\zeta$ -Ophiuchi. An <sup>a</sup> denotes the astrometric parameters came from Hoogerwerf et al. (2001). A <sup>b</sup> denotes the data came from Kirsten et al. (2015). The only differences between these two tests were the  $\mu$  and  $\pi$  parameters. A <sup>c</sup> denotes the data is from van Leeuwen (2007), and again the only differences are the  $\mu$  and  $\pi$  parameters. The position and characteristic age used for B1929 + 10 were the same in all of our tests, as was the position in RA and Dec for  $\zeta$ -Ophiuchi.

We see that in general there is good agreement between the three different models. Our results are between the numbers obtained by Hoogerwerf et al. (2001) and Kirsten et al. (2015) in the first simulation and only slightly different from Kirsten et al. (2015) in the last two simulations. We attribute part of our variation to random error in the Monte Carlo method, which we find to be  $\sim 0.01\%$ . This comes from running multiple Monte Carlo simulations of the same pulsar pair and finding the difference in the number of successful trajectories between simulations. It is possible there are other variations between the three models though, such as the Galactic potential, the solar motions used, or  $R_o$  and  $v_o$  which could contribute to these discrepancies. We note that the discrepancies between Hoogerwerf et al. (2001) and Kirsten et al. (2015) is larger than our discrepancies with Hoogerwerf et al. (2001), suggesting that our model is successful.

Table 4  
Number of Successes for B1929 + 10 and  $\zeta$ -Ophiuchi

Year of Parameters According to Citation	Hoogerwerf et al. (2001) Total	Hoogerwerf et al. (2001) Within US	Kirsten et al. (2015) Total	Kirsten et al. (2015) Within US	Our Model Total	Our Model Within US
B1929+10 (2001) $\zeta$ -Ophiuchi (2001)	30822	4214 (0.14%)	37521	6816 (0.23%)	33242	5529 (0.18%)
B1929+10 (2001) $\zeta$ -Ophiuchi (2007)			82840 (2.7%)	8	100109 (3.3%)	0
B1929+10 (2015) $\zeta$ -Ophiuchi (2007)			258272 (8.6%)	0	246270 (8.0%)	0

Table 4: The results of the three sets of trajectory trace backs for B1929 + 10 and  $\zeta$ -Ophiuchi using different sets of astrometric parameters. We report the number of orbits that had minimum separations of  $\leq 10$ , or “successes”, pc between just B1929 + 10 and  $\zeta$ -Ophiuchi in the “Total” columns. In the columns labeled “Within US” we report the number of orbits that had minimum separations of  $\leq 10$  pc between B1929 + 10 and  $\zeta$ -Ophiuchi *and* the Upper Scorpius (US) region.

When we look at the simulations using the most recent astrometric parameters for B1929 + 10, Kirsten et al. (2015) notes that most of the minimum separations were about 0.5 Myr ago and the smallest separation was 2.4 pc. The closest either B1929 + 10 or  $\zeta$ -Ophiuchi came to the center of the Upper Scorpius Region, Sco OB2, was 17 pc. Our model resulted in all of our successful trajectories occurring between 0.25 and 1 Myr, with neither the pulsar nor the star getting closer than 16 pc to Sco OB2. Similarly, we find that our minimum separation between B1929 + 10 and  $\zeta$ -Ophiuchi is 3.5 pc. These specific results agree very well so can conclude that for this particular well-studied pair of objects our model holds. However since the goals of this work are to look at pulsars with a common origin, we now analyze a pulsar pair that has been traced back to a common

origin, B2020 + 28 and B2021 + 51.

### 3.2 B2020+28 and B2021+51

Similar to our comparison of B1929 + 10 and  $\zeta$ -Ophiuchi, we will compare the Monte Carlo trace back algorithm on the pulsars B2020 + 28 and B2021 + 51. We use the parameters (Brisken et al., 2002, Kirsten et al., 2015) found in Table 5, and the same three-part Staekel Potential and appropriate radial velocity PDFs described above. We present our results along with those of the two different simulations, one using the parameters from Vlemmings et al. (2004) and the other using parameters from Kirsten et al. (2015) in Table 6. We do not compare the pulsar pair to a particular region. Thus we only look at the number of separations of  $\leq 10$  pc between B2020 + 28 and B2021 + 51.

Table 5

B2020 + 28 and B2021 + 51 Astrometric Data

Name	RA	Dec	$\mu_\alpha$	$\mu_\delta$	$\pi$	Dist	$\tau$
	(J2000)	(J2000)	(mas yr <sup>-1</sup> )	(mas yr <sup>-1</sup> )	(mas)	(kpc)	(Myr)
B2020 + 28 <sup>a</sup>	20 22 37.0718	28 54 23.0300	-4.38 $\pm$ 0.53	-23.59 $\pm$ 0.26	0.37 $\pm$ 0.12	2.7 <sup>+1.3</sup> <sub>-0.7</sub>	2.87
B2021 + 51 <sup>a</sup>	20 22 49.8655	51 54 50.3881	-5.23 $\pm$ 0.17	11.54 $\pm$ 0.28	0.50 $\pm$ 0.07	2.0 <sup>+0.3</sup> <sub>-0.2</sub>	2.74
B2020 + 28 <sup>b</sup>	20 22 37.06758	28 54 22.7563	-3.34 $\pm$ 0.05	-23.65 $\pm$ 0.11	0.72 $\pm$ 0.03	1.63 <sup>+0.50</sup> <sub>-0.23</sub>	2.87
B2021 + 51 <sup>b</sup>	20 22 49.85890	51 54 50.5005	-5.08 $\pm$ 0.42	10.84 $\pm$ 0.25	0.80 $\pm$ 0.11	1.28 <sup>+0.10</sup> <sub>-0.12</sub>	2.74

Table 5: Astrometric parameters for the two pulsars B2020 + 28 and B2021 + 51. An <sup>a</sup> denotes the parameters came from Brisken et al. (2002). A <sup>b</sup> denotes the parameters came from Kirsten et al. (2015). The positions is in RA and Dec using the J2000 coordinate system. Our characteristic ages come from PSRCAT (Manchester et al., 2005).

Table 6

Number of Successes for B2020 + 28 and B2021 + 51

Parameters	Vlemmings et al. (2004)	Kirsten et al. (2015)	Our Model
(Year)	(Total Successes)	(Total Successes)	(Total Successes)
2004	$\approx 0.15\%$	0.14%	2558 (0.08%)
2015		1866 (0.06%)	2201 (0.07%)

Table 6: The results of the two trace backs for B2020 + 28 and B2021 + 51. The number of successful trajectories of all three models using parameters from Brisken et al. (2002) are shown in the first row. The number of successes using the parameters from Kirsten et al. (2015) are shown in the second row.

We can see in Table 6 that using the parameters from Brisken et al. (2002), Kirsten et al. (2015) is able to obtain similar results as Vlemmings et al. (2004), but our results are very different. While the random error in the Monte Carlo Method, as described in section 3.1, along with possible differences in Galactic potential, solar motions, and other implementation variables, could contribute to the apparent error, they cannot account for a 0.07% difference. This simulation is the only one where we were unable to successfully reconstruct the radial velocity PDF used. We believe that this significant difference is due to mostly to our inability to reconstruct the radial velocity distributions of Vlemmings et al. (2004). This suggests that the radial velocity distribution has a large effect on the results of trajectory simulations for pulsars and thus that being able to more precisely constrain the  $V_r$  for pulsars is very important if we want to find their birth sites.

We also attempted to replicate the Kirsten et al. (2015) trajectory trace back of B2020 + 28 and B2021 + 51 using the new astrometric parameters and find our results to be in reasonable agreement. Kirsten et al. (2015) found that their successful trajectories

crossed within 10 pc about  $1.16_{-0.17}^{+0.18}$  Myr ago with a minimum separation of 1.9 pc. We obtain a similar number of trajectories crossing within 10 pc about  $1.16_{-0.17}^{+0.18}$  Myr ago with a minimum separation of 0.4 pc. Our minimum separation is lower than that obtained by Kirsten et al. (2015), however our results are generally in good agreement and the 0.01% difference is easily explained by the systematic error in the Monte Carlo Method.

We were successfully able to replicated 4 of the 5 pulsar trace back simulations described above. While we failed to replicate the results of Vlemmings et al. (2004) due to our inability to replicate the  $V_r$  PDF, we can be confident that our model can accurately trace back a pulsar through a galactic potential to locate a potential birth site.

## 4 Results of PSRPI Trajectories

We have simulated the trajectories of the 44 pulsars and 36 OB regions of interest. We first looked at all 1128 possible pairs of pulsar trajectory clouds, as in Figure 4, to determine the likelihood of common origins. We noted the pulsar trajectory clouds that intersected, as in Figure 4, at approximately the same time, as shown by the color scale. After looking at all possible pairs of pulsars, we looked at all 1584 of the combinations of pulsars and regions and analyzed it similarly. An example of a pulsar trajectory cloud with an OB region trajectory cloud is shown in Figure 10. We then analyzed these results to see if any pulsars that likely came from the same region also had intersecting trajectory clouds. Of the 1128 possible pulsar pairs, we found 16 that had the greatest likelihood to have come from the same region at the same time. In each pair the pulsars had similar characteristic ages and also similar ages to the OB region they were associated with. Due to computational constraints we discuss only one such pair, J0102 + 6537 and J0357 + 5236.

In addition to determining pulsars that may have a common origin, we look at likely birth regions for all 44 pulsars individually as in Figure 10. We have identified likely OB birth OB regions for 19 of the 44 pulsars within one of our 36 OB regions. We will discuss only one of these associations, the pulsar J0055 + 5117 with the OB region Cas OB2.

### 4.1 Pulsar Pairs from the Same OB Region: J0102+6537 and J0357+5236

We first discuss a pair of pulsars that we determined to have a likely common origin: J0102 + 6537 and J0357 + 5236. We use the same criteria for identifying a successful trajectory as in Vlemmings et al. (2004) and Kirsten et al. (2015), as described in Chapter

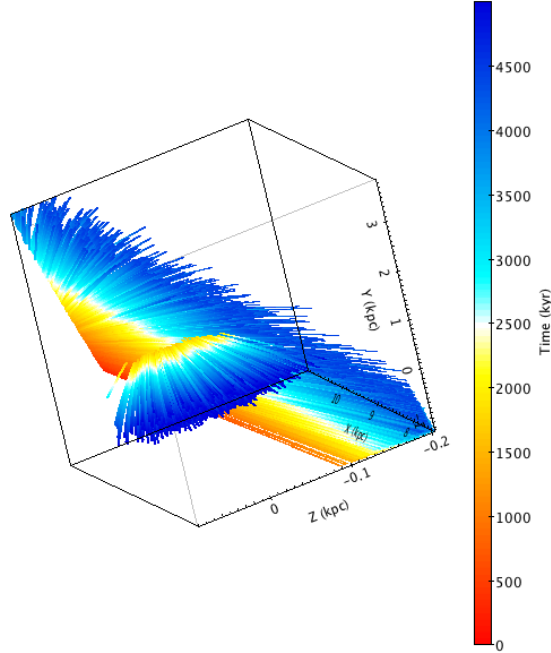


Figure 10: A close up of two example trajectory clouds using the pulsar J0102 + 6537 and the OB region Cas OB2. The Cas OB2 trajectory cloud is the smaller cloud coming out of larger pulsar trajectory cloud. This shows the two trajectory clouds overlapping at about the same time which suggests that the pulsar may have originated in this region. The x, y and z axes are in kpc as measured from the GC. The colors indicate time, where the scale is in kyr backwards from the present, so 1000 kyr is the same as being traced back for 1 Myr.

2. We report the number of successful orbits along with the parameter distribution and the Kolmogorov-Smirnov (KS) statistics comparing the distribution of successful trajectory parameters to the overall distribution of Monte Carlo selected parameters for the 1750 trajectories.

The trajectory clouds of these two pulsars are shown in Figure 11 and suggest a common origin since we have a clear intersection and the colors corresponding with time line up. We find that 1092, or 0.035%, of our orbits result in separations of 10 pc or less. This is a small number of successful trajectories when compared to the 30822 successful trajectories obtained by Hoogerwerf et al. (2001) and  $\approx 0.15\%$  successful trajectories ob-

tained by Vlemmings et al. (2004). We also look at the successful parameter distributions compared to the overall parameter distributions for J0102 + 6537 and J0357 + 5236 shown in Figures 12 and 13, respectively. The KS statistic for each parameter of each pulsar is shown in Table 7 along with the pulsar’s characteristic age.

Table 7

J0102 + 6537 and J0357 + 5236 KS Statistics and Age

Name	$\pi$	$\mu_\alpha$	$\mu_\delta$	$\tau$ (Myr)
J0102+6537	0.0605	0.0194	0.0407	4.42
J0357+5236	0.2152	0.0315	0.0370	6.55

Table 7: The KS statistics for the successful trajectory parameter distributions against the overall trajectory parameter distributions for J0102 + 6537 and J0357 + 5236. We look at just the KS statistics for  $\pi$  and  $\mu$ . Smaller KS values denote better correlation between the two distributions. We also list  $\tau$ , in Myr, of each pulsar again for reference.

The KS statistic is the difference between the two distributions of parameters if they had come from two separate PDFs. That is, a small KS value means there is a small difference between the two PDFs and they are close to the same. In the context of this work, this is the likelihood that our successful trajectories have the same parameter distributions as the overall parameter distributions. This allows us to statistically determine if the successful trajectory parameters are skewed from the measured values of  $\pi$  and  $\mu$ . For most parameters we obtain a low KS statistic showing that our successful trajectory results follow the measured parameters well, suggesting that the successful pairs show a realistic birth scenario. The only large KS statistic is for the parallax of J0357 + 5236. This tells us that for us to obtain a successful trajectory pair for J0102 + 6537 and J0357 + 5236, the  $\pi$  value for J0357 + 5236 is more likely to be larger than the mean, or

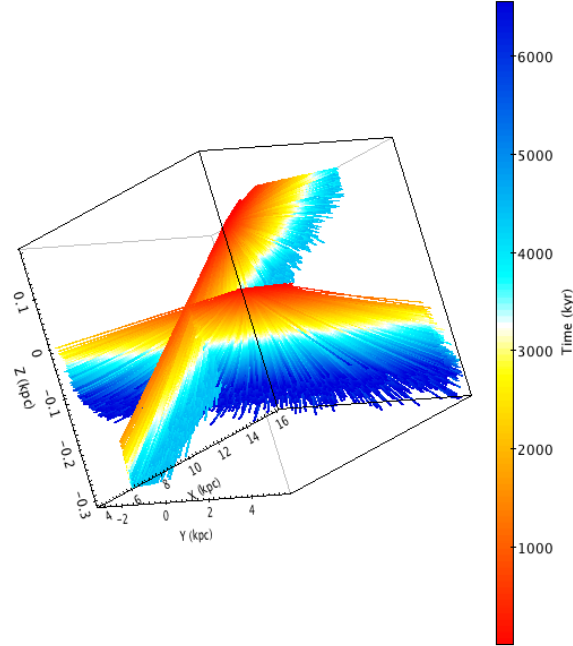


Figure 11: The trajectory clouds of J0102 + 6537 and J0357 + 5236. This shows the two trajectory clouds overlapping at about the same time which suggests a common origin is possible. The x, y and z axes are in kpc from the GC. Color indicates time, where the scale is in kyr backwards from the present, thus 1000 kyr is the same as being traced back for 1 Myr.

measured, value of  $\pi$  used in our PDF. We do not compute a KS statistic for  $V_r$  because we have no observational measurements for the radial velocity. Instead, the comparison of radial velocity distributions shows us the particular distribution of radial velocities necessary for two pulsars to have a separation of  $\leq 10$  pc apart.

The pulsar pair J0102 + 6537 and J0357 + 5236 show an interesting trend in their successful trajectory  $V_r$  distributions. Figures 12 and 13 show that both J0102 + 6537 and J0357 + 5236 must have strictly positive  $V_r$  values for a separation of less than 10 pc between the two to occur at any time. This suggests that if these pulsars did have a common birth location they are both currently moving away from us. While the right side of the red histogram shows a tail in these  $V_r$  distributions reaching velocities over 1000

J0102+6537 Parameter Distribution

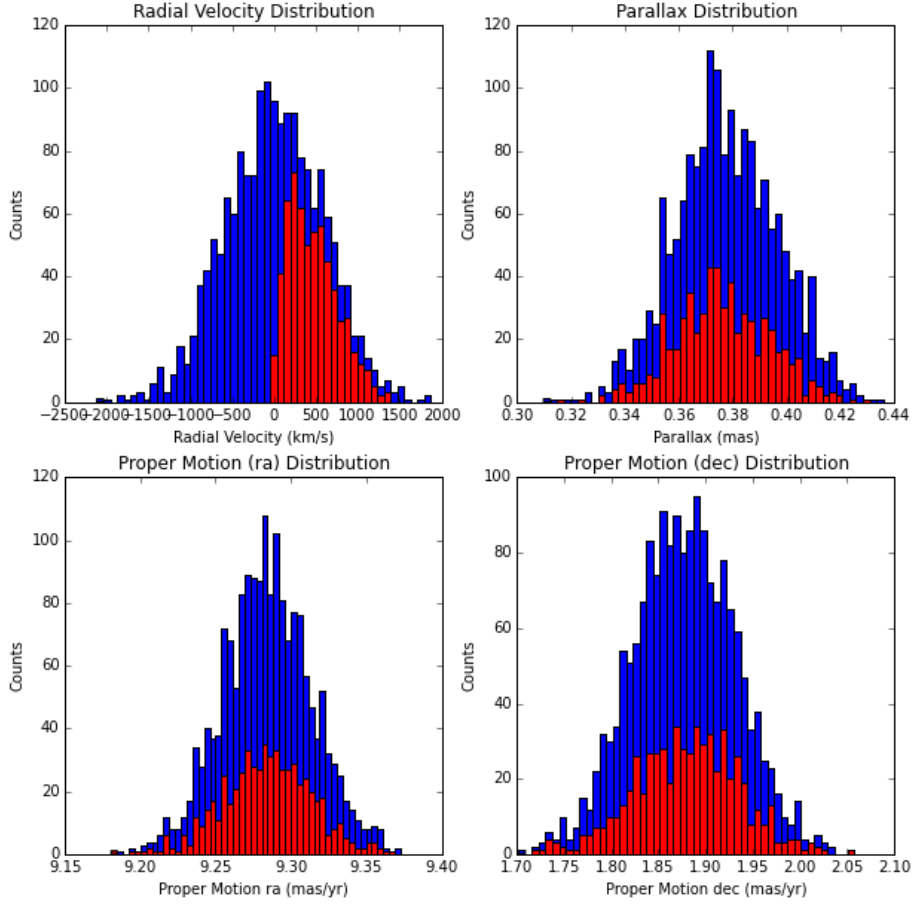


Figure 12: The Gaussian parameter distributions generated for J0102 + 6537 from our Monte Carlo Method. The blue histograms are the overall parent distributions of the parameters for all 1750 trajectories. The red histograms are the distributions of the parameters for the successful trajectories. We see the  $V_r$  distribution in the upper left,  $\pi$  in the upper right,  $\mu_\alpha$  in the lower left, and  $\mu_\delta$  in the lower right.

J0357+5236 Parameter Distribution

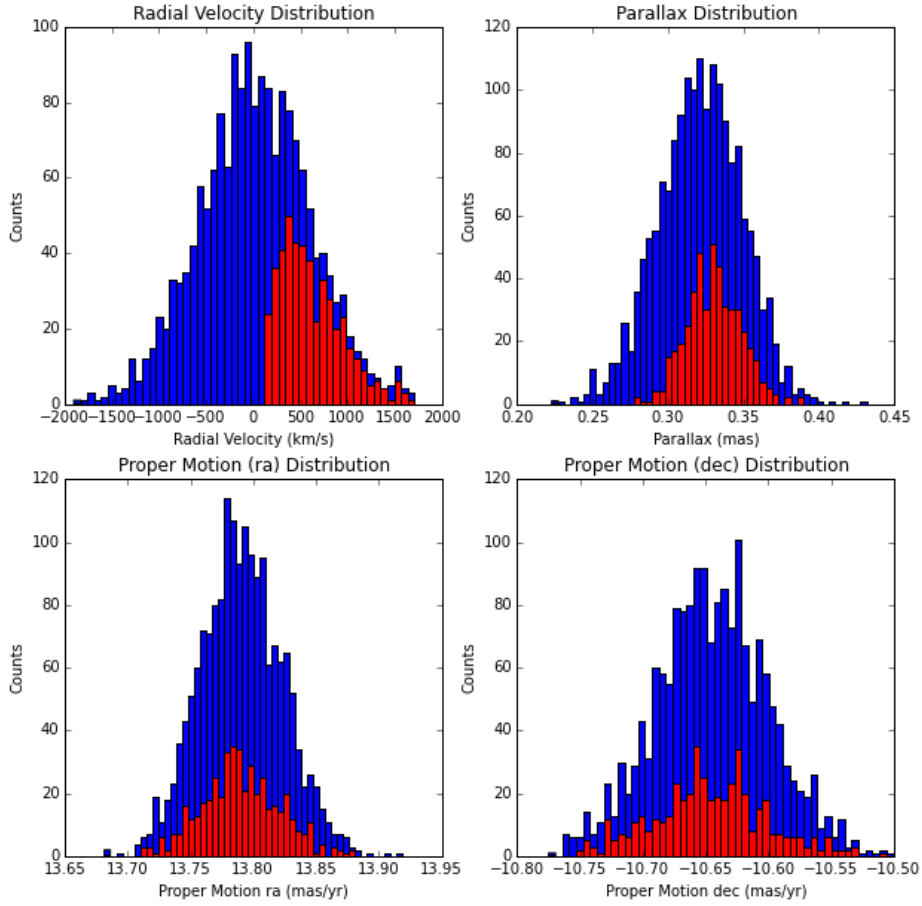


Figure 13: The Gaussian parameter distributions generated for J0357 + 5236 from our Monte Carlo Method. The blue histograms are the overall distributions of the parameters for all 1750 trajectories. The red histograms are the distributions of the parameters for the successful trajectories. The parameter distributions are the same as those in Figure 12.

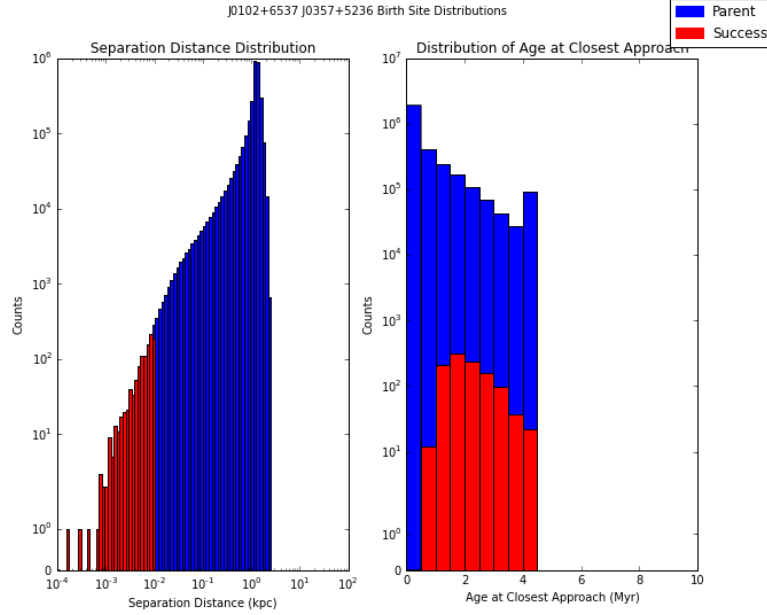


Figure 14: The left histogram shows the distribution of minimum trajectory separations for all 3 million possible orbits of J0102 + 6537 and J0357 + 5236. The blue shows every minimum separation less than 1 kpc, and the red shows the separations  $\leq 10$  pc. The right histogram shows the distribution of the time in the trajectory at which the minimum separation between J0102 + 6537 and J0357 + 5236 occurred.  $\tau$  for each pulsar is reported in Table 7. The blue shows the time at which the minimum separation occurred for all 3 million pairs, the red shows the time in the orbit at which the minimum separation occurred for pairs that had separations  $\leq 10$  pc.

$\text{km s}^{-1}$  they peak at about  $250 \text{ km s}^{-1}$  and  $300 \text{ km s}^{-1}$  for J0102 + 6537 and J0357 + 5236 respectively. This shows us that if both of these pulsars did have a common birth OB region, the most likely successful trajectories have radial velocities within a reasonable range ( $\sim 100$ 's  $\text{km s}^{-1}$ ). If we infer that these pulsars are from the same origin, we can then constrain  $V_r$  in future trajectory projections and simulations.

We also look at the distribution of the times at which the closest approaches of J0102 + 6537 and J0357 + 5236 occur. The right side of Figure 14 shows the distribution of the ages of the pulsars at every closest approach compared to the distribution of the

age of the pulsars when the closest approach was  $\leq 10$  pc. Here we note that most of the closest approaches occurred between 1 – 4 Myr, with more than half between 1 – 3 Myr. When we compare this time range with the characteristic ages of the pulsars, we see that 3 Myr is less than  $\tau$  for J0102 + 6537 (4.47 Myr) and about half of  $\tau$  for J0357 + 5236 (6.55 Myr). Since we know that  $\tau$  is an imprecise way to measure the age of pulsar, this does not immediately rule out a common origin for J0102 + 6537 and J0357 + 5236. However, we would expect to find the time of closest approach to be closer to  $\tau$  for both pulsars for a true common origin (Vlemmings et al., 2004).

Finally, we compare J0102 + 6537 and J0357 + 5236 to the Cas OB2 region. We find that 5710 of J0102 + 6537’s trajectories were within 10 pc of Cas OB2 at some point in time, with the smallest separation being 0.04 pc. However, we find that only 21 of J0357 + 5236’s trajectories are within 10 pc of Cas OB2 at some point in time, with the smallest separation being 1.5 pc. These separation distributions are shown in Figure 15. We also find that neither J0102 + 6537 nor J0357 + 5236 were both within 10 pc of Cas OB2 at the same time. The low number of successful J0357 + 5236 trajectories, along with the fact that we obtained no successful pairs of trajectories, show that it is highly unlikely that J0102 + 6537 and J0357 + 5236 share a common origin in the Cas OB2 region.

The fact that J0102 + 6537 had 5710,  $\approx 0.19\%$ , successful trajectories and a minimum separation of 0.04 pc from the center of Cas OB2 suggests that J0102 + 6537 may have been born in Cas OB2. This number is similar to the number of successful trajectories in both Vlemmings et al. (2004) and Hoogerwerf et al. (2001). However, if we look at Figure 16, we see that all of the closest passes occurred between 1 and 2.5 Myr ago, which is less than half of  $\tau$  (4.47 Myr) for J0102 + 6537, and a quarter of the approximate age (10 Myr) of Cas OB2. This leads us to two possible scenarios.

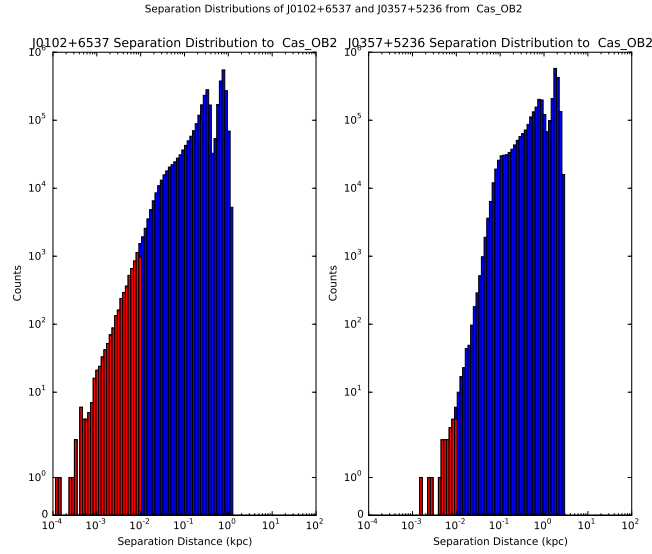


Figure 15: The histogram on the left shows the distribution of minimum separations less than 1 kpc between J0102 + 6537 and Cas OB2. The blue histogram shows the parent distribution of all minimum separations for all trajectory pairs, while the red shows the distribution for pairs with minimum separations  $\leq 10$  pc. The distributions on the right show the same results between J0357 + 5236 and Cas OB2.

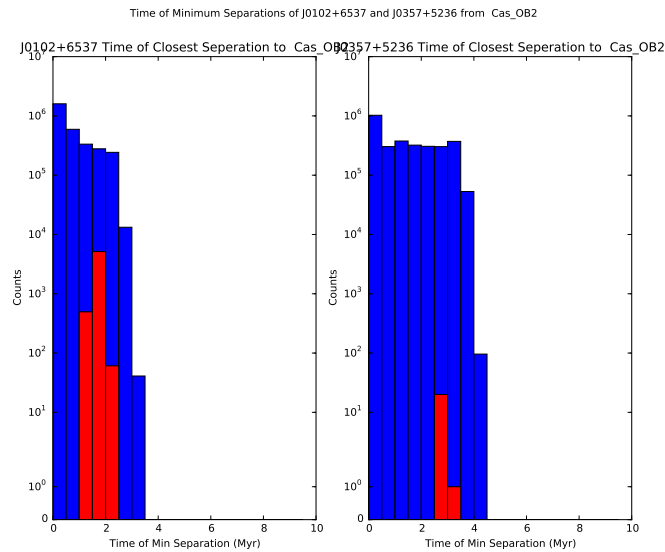


Figure 16: The histogram on the left shows the distribution of the time in the trajectory at which the minimum separation occurred between J0102 + 6537 and Cas OB2. The blue histogram shows the time distribution of minimum separations for all trajectory pairs, while the red shows the time at which the a minimum separation of  $\leq 10$  pc occurred between J0102 + 6537 and Cas OB2. The distributions on the right show the same results for J0357 + 5236 and Cas OB2.

The first scenario involves assuming that the characteristic age of J0102 + 6537 is incorrect. If J0102 + 6537 is actually closer to 2 Myr old, then we can conclude that Cas OB2 is the likely birth region of J0102 + 6537. The average lifetime of large O and B stars is on the order of a few million years (Stothers, 1966). The ages of Cas OB2 and J0102 + 6537 suggest that it is likely that a large O or B star formed in Cas OB2 about 10 Myr ago, and could easily have exploded in a supernova a few million years ago (Maeder & Meynet, 2000) producing a pulsar which is given a kick about 2.5 Myr ago. If the progenitor star has a lifetime of only about 2 Myr (Savedoff, 1956) we could consider 8 Myr as an upper limit on the age of J0102 + 6537. The most likely birth scenario for J0102+6537, therefore, is that a large O-type star in Cas OB2 exploded in an asymmetric supernova about 5 – 8 Myr ago, and the core collapsed into a pulsar, J0102 + 6537, that was then kicked out of the region (Dewey & Cordes, 1987) only 2.5 Myr ago.

The second scenario is that  $\tau$  for J0102 + 6537 is correct and the pulsar was not born in Cas OB2. This also has interesting implications, since it is still likely that J0102+6537 came near Cas OB2  $\sim$  2 Myr ago. This would mean that J0102 + 6537 passed through the Cas OB2 region. It is then possible that J0102 + 6537 may have had some kind of interaction with another star in Cas OB2. Depending on the strength of this interaction, the initial trajectory of J0102 + 6537 could have been altered. If there were a supernova in the time that J0102 + 6537 passed through Cas OB2, J0102 + 6537 could have been shot out of Cas OB2 imparting a large velocity to the pulsar (Iben & Tutukov, 1996).

There is no strong evidence to support either scenario to account for the past history of J0102+6537 in our simulation, but it still presents interesting astrophysical possibilities for stellar evolution. The likelihood of either of these scenarios is not well studied for pulsars, and further studies of J0102 + 6537 and Cas OB2 as well as other similar pulsars will allow us to learn more about the general population of neutron stars as well as

supernova dynamics.

Since it is unlikely that J0102 + 6537 and J0357 + 5236 had a common origin in Cas OB2, we cannot use the successful trajectories shown in Figure 12 to limit J0102 + 6537 to just positive radial velocities. We were also unsuccessful in determining a birth region for J0357 + 5236 in our model. We were, however, able to determine a possible birth location for J0102 + 6537 and explore possible birth scenarios, although we are unable to constrain the radial velocity parameter for J0102 + 6537. Through our analysis of this pair we have shown that our method works well for determining which pairs of pulsars and regions to analyze computationally.

## 4.2 Pulsar Pairs with No OB Region Matches

In our preliminary visual analysis of our pulsar trajectory clouds we also find 4 other pulsars had possible common origins with other pulsars but did not have likely births within our sample of OB regions. Table 8 lists these pulsars and their potential matching pulsars. While we were not able to analyze these pulsars for likelihood of a common origin, there are a few conclusions we can draw from this.

One possible reason for these apparent matches is that our first visual analysis was a statistical coincidence due to the number of trajectories generated and uncertainties in the initial parameters. If this is the case then these pulsars would not have any separations less than 10 pc away from each other at the same time. Another consideration is that the two pulsars do share a common origin, but that their progenitor stars were in an isolated environment, possibly in a binary system with each other. However, while O stars can be ejected from clusters, most are found within OB associations (Oh et al., 2015) so we reject this scenario. The third possibility is that, even if the two pulsars do not share

a common origin, these pulsars originated in OB associations that are not within our sample, which include only 36 of 140 different OB associations from Tetzlaff et al. (2010).

Table 8

Potential Pulsar Pairs without Associated Regions

Unassociated Pulsar	Potential Pulsar Match
J0040+5716	J1257-1027
	J1321+8323
J0826+2537	J1937+2544
	J2113+2754
	J2325+6316
J1257-1027	J1321+8323
	J1607-0032
	J2149+6329
J1919+0021	J0055+5117

Table 8: Pulsar pairs that were identified as possibly having a common origin but were not found to have an association with any OB region from Table 2. Further analysis on the other 104 OB associations (Tetzlaff et al., 2010) not analyzed in this work and these 4 pulsars is required before any final conclusions about their origins can be made.

### 4.3 Pulsar Birth OB Regions: J0055+5117 and Cas OB2

We also use our method to determine if we can associate a pulsar with an OB association as with J0102 + 6537 and Cas OB2. By looking at a pulsar trajectory cloud and a region trajectory cloud, we can deduce if it is likely that the pulsar was born in that region, as in Figure 10. Our analysis of pulsar birth OB regions is even more useful than looking

at the trajectory clouds of two pulsars together. If we are able to determine the birth locations of many pulsars we can then see which pulsars were born in the same OB region and use their characteristic ages together with the pulsar trajectory clouds, as in Figure 4, to determine the probability that the two pulsars could have related progenitor stars (Vlemmings et al., 2004). This would reduce the number of pulsar pair trajectory clouds that must be analyzed since we could determine that only certain pairs could have been born within the same OB region. While we determined many likely pulsar birth regions, due to computational restraints, we have only one relation to discuss at the time of this writing.

One pulsar-OB region association suggested in our visual analysis was that of the pulsar J0055 + 5117 and the OB region Cas OB2, whose trajectory clouds are both shown in Figure 17. J0055 + 5117 has a  $\tau = 3.51$  Myr, well within the age ( $\sim 10$  Myr) of Cas OB2, further suggesting J0055 + 5117 could have been born in Cas OB2. When we compute the actual separations between the trajectories of J0055 + 5117 and Cas OB2, we find only 3 successful trajectories with separations less than 10 pc, and a minimum separation of 5.2 pc. The distribution of separations between J0055 + 5117 and Cas OB2 less than 1 kpc are shown on the left side of Figure 18. We see from the right side of Figure 18 that the time at which these 3 separations between J0055 + 5117 and Cas OB2 occurred was between 1 – 1.5 Myr ago. None of the minimum trajectory pair separations occur later than 2 Myr ago, which is less than the characteristic age of J0055 + 5117. While we know that  $\tau$  is imprecise, we expect many of the minimum separations between two objects to occur nearer to the  $\tau$  of the pulsar in question if it is likely to have been born in that region. Additionally, just 3 successful trajectories is a value smaller than the systematic differences in the Monte Carlo method itself. These results show that it is extremely unlikely that J0055 + 5117 was born within the Cas OB2 association. We

did not find it likely that J0055 + 5117 was born within another cluster of OB stars in our sample of 36 OB associations. However, we note that there are 104 OB regions in the sample analyzed by Tetzlaff et al. (2010) we did not analyze.

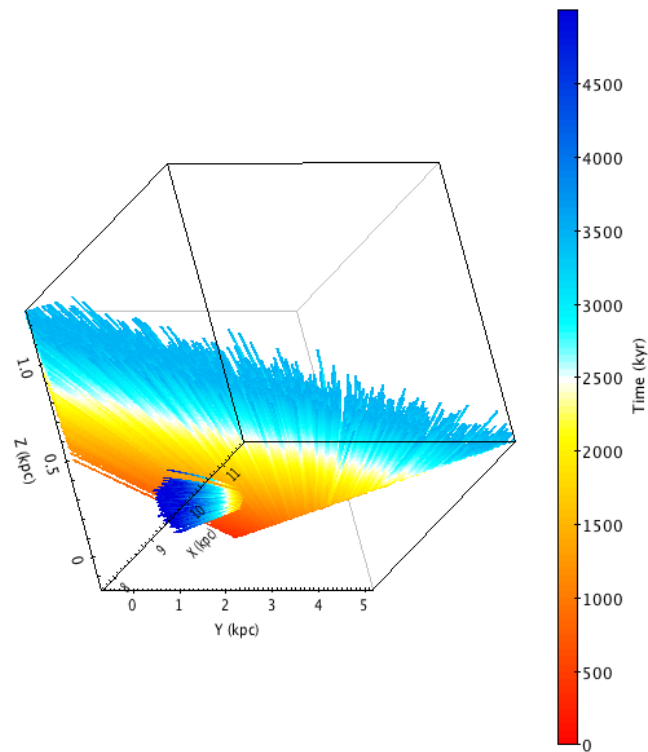


Figure 17: The large, fan-shaped trajectory cloud for the pulsar J0055 + 5117 and the cone-shaped trajectory cloud of the Cas OB2 region. This shows the two trajectory clouds overlapping at about the same time which suggests that it is possible J0055 + 5117 could have been born in the Cas OB2 region. The x, y and z axes are in kpc as measured from the GC. Color indicates time, where the scale is in kyr backwards from the present, thus 1000 kyr is the same as being traced back for 1 Myr.

Separation Distribution of J0055+5117 from Cas\_OB2

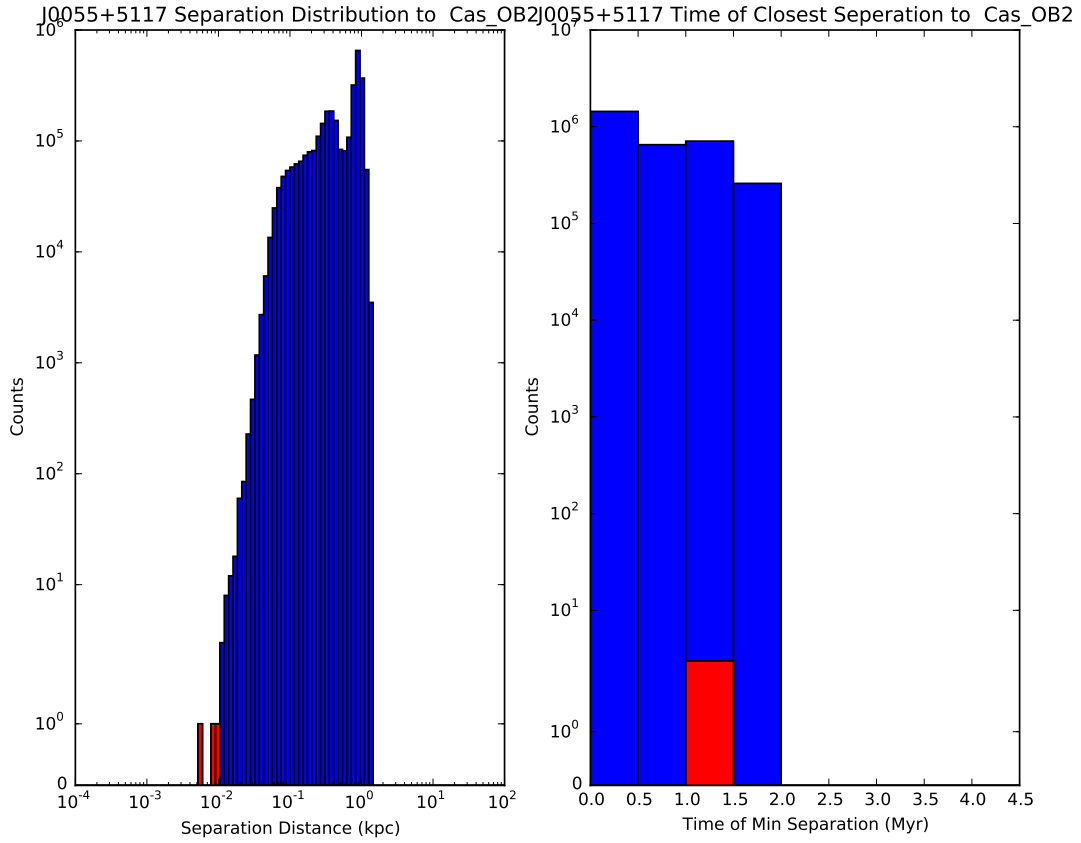


Figure 18: The left histogram shows the distribution of minimum trajectory separations for all 3 million possible orbits of J0055 + 5117 and Cas OB2. The blue shows every minimum separation less than 1 kpc, and the red show the separations  $\leq 10$  pc. The right histogram shows the distribution of the time in the trajectory that the minimum separation between J0055 + 5117 and Cas OB2 occurred. The blue shows the time at which the minimum separation of every trajectory pair occurred, the red shows the time in the orbit of the minimum separation for pairs that had separations  $\leq 10$  pc. This shows that all of the minimum separations of the 3 million orbits occurred  $\leq 2$  Myr ago. Particularly the three separations of  $\leq 10$  pc all occurred between 1 – 1.5 Myr ago.

## 5 Conclusions

We have used our model to successfully trace back the trajectories of 44 pulsars in the PSRPI survey and visually determine if they were likely to have a common origin. We also traced back the trajectories of 36 OB regions and similarly visually determined the likelihood that one of our pulsars had a likely origin in one of these OB regions. While our model is only applicable for pulsars with  $\tau \lesssim 30$  Myr, this accounts for about 75% of the PSRPI survey and a large number of pulsars that have already been discovered. Our model is thus likely to be very useful for future studies looking into the determining the birth regions of pulsars. As more astrometric measurements of young pulsars are gathered we will be able to determine the likely birth regions of more pulsars. This in turn can be cross correlated with previous pulsar-OB region associations. It will then be possible, also using our model, to determine the likelihood that any pulsars coming from the same OB region were associated with each other, or had progenitor stars associated with each other, as in Vlemmings et al. (2004).

We were able to confirm the validity of our model, comparing it with previous results from Hoogerwerf et al. (2001) and Kirsten et al. (2015) concerning B1929 + 10 and  $\zeta$ -Ophiuchi and from Vlemmings et al. (2004) and Kirsten et al. (2015) concerning B2020 + 28 and B2021 + 51. Our comparisons returned similar numbers of successful trajectories for both pairs of objects with the exception of Vlemmings et al. (2004). However, our inability to replicate exactly the results of Vlemmings et al. (2004) shows the importance of the  $V_r$  probability density function (PDF) used when tracing back pulsar trajectories, since this was also the only simulation where we were not able to replicate the  $V_r$  PDF exactly. Thus, being able to constrict the radial velocity of a pulsar is a critical part of being able to determine an exact birth location of that pulsar. While the wide Gaussian

$V_r$  PDF shown in Figure 3 allows us to account for the most reasonable values for a pulsar's radial velocity, it does not allow us to easily constrict the radial velocity of a pulsar.

While we were not able to fully analyze every likely pulsar pair association or pulsar-birth region association due to computational restraints, our analysis of the pulsars J0102 + 6537 and J0357 + 5236 and the pulsar-OB region pair J0055 + 5117 and Cas OB2 show promise for future studies. While J0102 + 6537 and J0357 + 5236 were not found to have a common origin in Cas OB2, and that J0102 + 6537 was not likely born in Cas OB2, we are able to propose two interesting possibilities for the history J0102 + 6537. Similarly, in our analysis of J0055 + 5117 and Cas OB2, we found that it is extremely unlikely that Cas OB2 is the birth region of J0055 + 5117. While we were unable to determine a likely birth region for J0055 + 5117 from our sample of 36 OB associations, we have narrowed down the possible birth regions for this pulsar. Through these two possible pairs, this work has shown that our method is useful in determining likely birth regions for pulsars.

The pulsars J0102+6537 and J0357+5236 and the pulsar-OB region pair J0055+5117 and Cas OB2 were just two comparisons that appeared to have promising results in our preliminary visual analysis of the trajectory clouds. There are many more pairs of pulsars and associated OB regions that suggested a common birth region for both pulsars that we were not able to further analyze in this work. These other pulsar pairs and pulsar-OB region associations can be found in Tables 9 and 10 respectively in Appendix A and will be analyzed in future work.

In addition to future analysis of the pulsar-pulsar and pulsar-OB region associations found in this initial study, there is much future work that can be done with the 44 PSRPI pulsars discussed in this work. Tetzlaff et al. (2010) looked at 140 different OB

associations as potential birth regions for just four young pulsars. Of these 140 different OB associations, we analyzed only 36, just about 25% of the number of potential birth OB regions we could have looked at. While this was due to computational constraints, 25 pulsars were found to have no likely birth OB regions within our sample of 36 OB associations. In future work an analysis of the other 104 OB regions in Tetzlaff et al. (2010) with the 44 pulsars of interest in this work could lead to determining the birth regions for these pulsars as well.

Furthermore, this analysis method can be performed on pulsars yet to be discovered and on pulsars with currently unknown astrometric parameters. We note as in Kirsten et al. (2015) that the methods for measuring the astrometric parameters of pulsars, stars, and even OB associations change and improve with the development of better techniques and more sensitive instruments. Our model and the implementation of the *Galpy* package allow us to easily recompute previously analyzed trajectories of astrophysical objects and compare new results to previous results, as in Kirsten et al. (2015).

The implementation of the *Galpy* package and our Monte Carlo Method also allows us to account for any future research in pulsar radial velocity PDFs, galactic potentials, solar motions, and measurements of our own position in the Milky Way relative to the Galactic Center. All of these measurements and models are utilized in our trace back method and are easy to change within the model itself. This allows our model to produce continually updated results while always using the most recent and accurate trajectory parameters. The versatility of our model to include the most recent scientific discoveries related to trajectory modeling allows it to be useful far into the future.

### *Acknowledgements*

I would first like to thank my advisors at Cornell, Jim Cordes and Shami Chatterjee, for helping me start this project and introducing me to world of pulsars. I would also like to thank the NSF and the Cornell Astronomy REU program for giving me the wonderful opportunity to work with Jim and Shami and the entire Astronomy Department. I would like to thank my Union advisor Greg Hallenbeck, who made sure I actually turned my thesis in. I would also like to thank Michael Warrenner, who helped me with various sundry computer and coding errors, and whose idea it was to use TOPCAT (Taylor, 2005) to look at the pulsar trajectory clouds. My gratitude and thanks also goes to the entire Union College Department of Physics and Astronomy for supporting me and helping me find my passion for this field.

This material is based upon work supported by the National Science Foundation Research Experience for Undergraduates program in Astronomy and Astrophysics at Cornell University under Grant No. NSF/ AST-1156780. The National Radio Astronomy Observatory is a facility of the National Science Foundation operated under cooperative agreement by Associated Universities, Inc. This work made use of the ATFN Pulsar Catalogue (Manchester et al., 2005) found at <http://www.atnf.csiro.au/people/pulsar/psrcat/>.

## 6 Appendix A

In this appendix we present the pairs of pulsars from the PSRPI survey identified to have a possible common origin that we were unable to analyze further than our preliminary visual trajectory cloud analysis in this work. The pulsar pairs along with the likely OB regions are presented in Table 9.

We also present the pulsars that were connected to a possible birth OB region from our sample of 36 OB associations that we were unable to further analyze. These pulsars and any likely OB region associations are shown in Table 10. Both of these sets of results show the success of our method in identifying possible pulsar pairs with a common origin and also possible pulsar birth OB regions, thus significantly lowering the time necessary for computations. We hope to analyze these results in the future.

Table 9

Common Origin Pulsar Pairs and Possible Birth OB Regions

Pulsar 1	Pulsar 2	Associated OB Region(s)
J0102+6537	J0629+2415	AB Dor
	J2113+2754	Cas OB2, Cep OB1
J1532+2745	J2113+4644	Ara OB1A
	J2317+2149	Ara OB1A
	J2325+6316	NGC 457
J0152-1637	J2248-0101	Cam OB3
	J2325+6316	Cam OB3
J1136+1551	J1623-0908	HD 141569
J1623-0908	J1645-0317	Sco OB1
	J1703-1846	Sco OB4
J1754+5201	J2317+2149	LCC
	J2317+2149	Ser OB1, UCL
J0357-5236	J1543-0620	Sgr OB4, Sct OB2, Ser OB1
	J1321+8323	Sgr OB5
	J1623-0908	Sgr OB5

Table 9: The pairs of pulsars from our sample of 44 from the PSRPI survey that upon visual trajectory cloud analysis appeared to have a common origin in the same OB region. These pairs were not further analyzed and are presented to show further results of our method and present the basis for future work.

Table 10  
Pulsar and Possible Birth OB Regions

Pulsar	Associated OB Region(s)
J0102+6537	Cep OB1
J0152-1637	Cas OB2, NGC 457
J0357+5236	NGC 6530, Sgr OB4, Sgr OB5
J0629+2415	AB Dor, Ext R CrA, Gem OB1, Her-Lyr
J1136+1551	Cen OB1
J1321+8323	Sgr OB5
J1532+2745	Ara OB1A
J1543-0620	Sgr OB4
J1607-0032	$\epsilon$ Cha
J1623-0908	Sco OB1
J1645-0317	Sco OB1
J1754+5201	AB Dor, Her-Lyr, UCL
J2113+4644	AB Dor, Ara OB1A
J2248-0101	Cam OB1, NGC 457
J2305+3100	Cas OB2
J2317+2149	AB Dor, Ara OB1A
J2325+6316	Col 121, NGC 457
J2354+6155	Cas OB2

Table 10: The pulsars that showed possible birth OB regions within our sample of 36 OB associations from Tetzlaff et al. (2010) that were not further analyzed in this work. These pairs represent a basis for future work.

## References

- Bisnovatyi-Kogan, G. S. 2006, *Physics Uspekhi*, 49, 53
- Brisken, W. F., Benson, J. M., Goss, W. M., & Thorsett, S. E. 2002, *ApJ*, 571, 906
- Bovy, J. 2015, *ApJS*, 216, 29
- Bovy, J., & Rix, H.-W. 2013, *ApJ*, 779, 115
- Campbell, R. M., Bartel, N., Shapiro, I. I., et al. 1996, *ApJ*, 461, L95
- Chatterjee, S., Vlemmings, W. H. T., Brisken, W. F., et al. 2005, *ApJ*, 630, L61
- Cordes, J. M. 1993, *Planets Around Pulsars*, 36, 43
- Damour, T., & Taylor, J. H. 1992, *Phys. Rev. D*, 45, 1840
- Davis, M. M., Taylor, J. H., Weisberg, J. M., & Backer, D. C. 1985, *Nature*, 315, 547
- de Zeeuw, P. T., Hoogerwerf, R., de Bruijne, J. H. J., Brown, A. G. A., & Blaauw, A. 1999, *AJ*, 117, 354
- Dejonghe, H., & de Zeeuw, T. 1988, *ApJ*, 333, 90
- Deller, A. T., Brisken, W. F., Chatterjee, S., et al. 2011, 20th Meeting of the European VLBI Group for Geodesy and Astronomy, held in Bonn, Germany, March 29-30, 2011, Eds: W. Alef, S. Bernhart, and A. Nothnagel, Institut für Geodäsie und Geoinformation, Rheinischen Friedrich-Wilhelms-Universität Bonn, p. 178-182, 178
- Dewey, R. J., & Cordes, J. M. 1987, *ApJ*, 321, 780
- Duncan, R. C., & Thompson, C. 1992, *ApJ*, 392, L9

- Famaey, B., & Dejonghe, H. 2003, MNRAS, 340, 752
- Ferrario, L., & Wickramasinghe, D. T. 2008, *Astrophysics of Compact Objects*, 968, 188
- Gillessen, S., Eisenhauer, F., Fritz, T. K., et al. 2009, ApJ, 707, L114
- Graham-Smith, F., & McLaughlin, M. A. 2005, *Astronomy and Geophysics*, 46, 1.23
- Gott, J. R., III, Gunn, J. E., & Ostriker, J. P. 1970, ApJ, 160, L91
- Hobbs, G., Lorimer, D. R., Lyne, A. G., & Kramer, M. 2005, MNRAS, 360, 974
- Hoogerwerf, R., de Bruijne, J. H. J., & de Zeeuw, P. T. 2001, A&A, 365, 49
- Hoyle, F., Fowler, W. A., Burbidge, G. R., & Burbidge, E. M. 1964, ApJ, 139, 909
- Hulse, R. A., & Taylor, J. H. 1975, ApJ, 195, L51
- Iben, I., Jr., & Tutukov, A. V. 1996, ApJ, 456, 738
- Jacoby, B. A., Cameron, P. B., Jenet, F. A., et al. 2006, ApJ, 644, L113
- Jenet, F., Finn, L. S., Lazio, J., et al. 2009, arXiv:0909.1058
- Kirsten, F., Vlemmings, W., Campbell, R. M., Kramer, M., & Chatterjee, S. 2015, A&A, 577, A111
- Kohler, S. 2015, AAS Nova Highlights, 248
- Lai, D., Chernoff, D. F., & Cordes, J. M. 2001, ApJ, 549, 1111
- Lam, M. T., Cordes, J. M., Chatterjee, S., et al. 2015, arXiv:1512.08326
- Lorimer, D. R. 2008, *Living Reviews in Relativity*, 11,

- Maeder, A., & Meynet, G. 2000, *ARA&A*, 38, 143
- Manchester, R. N., Hobbs, G. B., Teoh, A., & Hobbs, M. 2005, *VizieR Online Data Catalog*, 7245,
- Miyamoto, M., & Nagai, R. 1975, *ASJP*, 27, 533
- Navarro, J. F., Frenk, C. S., & White, S. D. M. 1996, *ApJ*, 462, 563
- Oh, S., Kroupa, P., & Pflamm-Altenburg, J. 2015, *ApJ*, 805, 92
- Richards, D. W., & Comella, J. M. 1969, *Nature*, 222, 551
- Savedoff, M. P. 1956, *ApJ*, 124, 533
- Schönrich, R. 2012, *MNRAS*, 427, 274
- Stairs, I. H., Thorsett, S. E., Taylor, J. H., & Wolszczan, A. 2002, *ApJ*, 581, 501
- Stothers, R. 1966, *ApJ*, 143, 91
- Tauris, T. M. 1994, *Proceedings of the Astronomical Society of Australia*, 11, 82
- Taylor, M. B. 2005, *Astronomical Data Analysis Software and Systems XIV*, 347, 29
- Taylor, J. H., & Manchester, R. N. 1977, *ARA&A*, 15, 19
- Taylor, J. H., Manchester, R. N., & Lyne, A. G. 1993, *ApJS*, 88, 529
- Tetzlaff, N., Neuhäuser, R., Hohle, M. M., & Maciejewski, G. 2010, *MNRAS*, 402, 2369
- Turolla, R., Zane, S., & Watts, A. L. 2015, *Reports on Progress in Physics*, 78, 116901
- van Leeuwen, F. 2007, *Astrophysics and Space Science Library*, 350,

Vlemmings, W. H. T., Cordes, J. M., & Chatterjee, S. 2004, *ApJ*, 610, 402

Weisberg, J. M., & Taylor, J. H. 2005, *Binary Radio Pulsars*, 328, 25